

From Causal Discovery to Intervention Simulation: Modeling Precariousness and Depression in the HELIUS Study

Kyuri Park ^{*1}, Leonie K. Elsenburg², Mary Nicolaou², Karien Stronks², Vítor V. Vasconcelos^{1,3}

¹*Computational Science Lab, Informatics Institute, University of Amsterdam, PO Box 94323, Amsterdam, 1090GH, the Netherlands*

²*Department of Public and Occupational Health, Amsterdam Public Health Research Institute, Amsterdam UMC, University of Amsterdam, Amsterdam, the Netherland*

³*Institute for Advanced Study, University of Amsterdam, Oude Turfmarkt 147, Amsterdam, 1012GC, the Netherland*

2025-08-25

Abstract

This study investigates how the internal structure of depression–precariousness dynamics shapes responsiveness to external support. Using cross-sectional data from the HELIUS study, we first apply cycle-capable causal discovery algorithms to estimate directional dependencies between financial stress, domain-specific precariousness, and depressive symptoms. Our multi-resolution analysis—spanning both aggregate and symptom-level constructs—highlights financial stress as a plausible upstream driver of depression, with symptoms such as sleep disturbance and depressed mood emerging as initiators of broader social vulnerability. To translate these structural insights into dynamic predictions, we construct a family of analytically calibrated linear stochastic models. Simulations reveal that variations in internal structure can substantially alter system responses to financial stress reduction. Some models show rapid but transient improvements in depression, while others adjust more slowly yet sustain gains over time. Precariousness tends to respond more immediately across all configurations, though its trajectory also shifts subtly with structural variation. Together, these findings demonstrate that intervention outcomes depend not only on the magnitude of external input but also on latent properties of the system. More broadly, this study illustrates how combining causal discovery with dynamical modeling supports principled, simulation-based exploration of intervention scenarios—grounded in data, yet able to probe counterfactual structure. This approach offers a scalable framework for diagnosing hidden system constraints and informing targeted public health strategies in complex psychosocial domains.

^{*}To whom correspondence should be addressed. k.park@uva.nl

1 Introduction

Mental health disorders represent a growing global health concern, especially in urbanized regions (Gruebner et al., 2017; World Health Organization, 2022). In 2019, one in eight people worldwide were living with a mental health condition, with the highest disability-adjusted life years (DALYs) due to mental and addictive disorders present in high-income countries such as those in Northern Europe, North America, and Australia (Rehm & Shield, 2019; World Health Organization, 2022). Despite growing awareness, governments have struggled to design effective responses. Mental health outcomes arise from complex, multi-level dynamics between the social, economic, and spatial structures of urban environments—making both diagnosis and intervention design deeply challenging (Van Der Wal et al., 2021).

Recent work has shifted focus from individual-level vulnerability to broader social and structural determinants. While high-income nations show elevated overall DALYs, within-country disparities reveal that income inequality is a significant predictor of mental health burden (Rehm & Shield, 2019). Moreover, precarious working conditions, housing instability, and neighborhood disadvantage have all been linked to increased risk of depression and anxiety (Fone et al., 2014; Pevalin et al., 2017; Rönnblad et al., 2019; Rugulies et al., 2023). This growing literature highlights that poor mental health is not merely a personal issue but one rooted in sustained socioeconomic stress and structural uncertainty.

Building on this, recent studies have introduced the concept of precariousness as a multidimensional condition characterized by instability and lack of control across several life domains, including employment, finances, housing, social relations, and cultural belonging (Elsenburg et al., 2025; McKee et al., 2017). This broader view reveals how different forms of insecurity can co-occur and compound, forming an ecosystem of risk. However, despite growing evidence of association between precariousness and mental health, a fundamental question remains unresolved: *How do these factors causally influence one another?* Most existing studies rely on cross-sectional correlations, leaving open questions about directionality and feedback. Without stronger causal insight, it remains difficult to identify priority targets for intervention or to anticipate and quantify intended and unintended effects.

This study aims to investigate the causal mechanisms linking precariousness and depression and how those mechanisms shape system responses to external intervention. Specifically, we ask: *How does the internal configuration of the precariousness-depression relationship affect the outcomes of stress-reducing interventions?* To answer this, we combine two approaches. First, we use cycle-capable causal discovery algorithms to infer directional relationships among domain-specific precariousness factors and depressive symptoms. By examining both aggregated measures (depression sum score and a composite precariousness index) and disaggregated variables (individual depressive symptoms and specific life-domain indicators), we capture broad patterns of relationship as well as fine-grained causal pathways. Second, we translate these insights into a computational dynamical model that simulates how depression and precariousness co-evolve under varying levels of external stress. This model enables us to probe how system properties—such as

feedback strength and stochastic noise—govern responsiveness to intervention. When the effects of depression symptoms onto the social precarity subsystem are weaker than the reverse path, there is higher sensitivity of depression to intervention, reflecting both a faster reduction post financial intervention but also quicker relapse once financial stresses are reestablished. By integrating causal discovery with dynamic simulation, we demonstrate that intervention strategies can be tailored to the underlying architecture of vulnerability.

2 Methods

2.1 Data

We use data from the HELIUS (HEalthy LIfe in an Urban Setting) study (Snijder et al., 2017; Stronks et al., 2013). It captures the diverse population of the city of Amsterdam by including the six main ethnic groups and provides comprehensive health and lifestyle data, including depressive symptoms as measured by the PHQ-9 (Galenkamp et al., 2017). To operationalize indicators of precariousness, we draw on the framework outlined in previous research (Elsenburg et al., 2025) and select a set of relevant variables. To ensure a robust representation of precariousness in our causal discovery models, we conducted exploratory analyses to identify consistent and meaningful data-driven factor structures. These analyses led to the identification of five distinct precariousness factors: three reflecting structural domains—employment, housing, and social relationships—and two capturing recent life stressors—financial and relational. Each factor is composed of multiple observed variables, as outlined below. Additional details on the HELIUS study and the factor extraction process are provided in the [Appendix](#).

- Employment precariousness: `emp_stat` (current employment status), `work_sit` (nature of work situation).
- Social precariousness: `soc_freq` (frequency of social contact), `soc_adq` (perceived adequacy of social support).
- Housing precariousness: `nb_safe` (neighborhood safety), `nb_res` (access to neighborhood resources), `nb_rent` (proportion of rental housing), `cul_rec` (availability of cultural resources).
- Recent relational stressors: `frd_brk12` (experience of a friendship breakup), `conf12` (recent interpersonal or relational conflict).
- Recent financial stressors: `fincril12` (experience of a financial crisis), `inc_diff` (difficulty managing household income).

Following data cleaning and normalization procedures, the analytical sample comprises 21,628 individuals. In addition to the five identified precariousness factors, we computed an overall precariousness score by summing these five factor scores, thereby capturing a composite measure of accumulated precariousness across domains. Depression is represented using the PHQ-9 (Kroenke et al., 2001), both as a total sum score and as individual symptom scores. In the subsequent causal discovery analysis, we explore the relationship between depression and precariousness using both aggregated scores and their disaggregated components. See Figure 1 for the overall distributions of the variables used in the analysis.

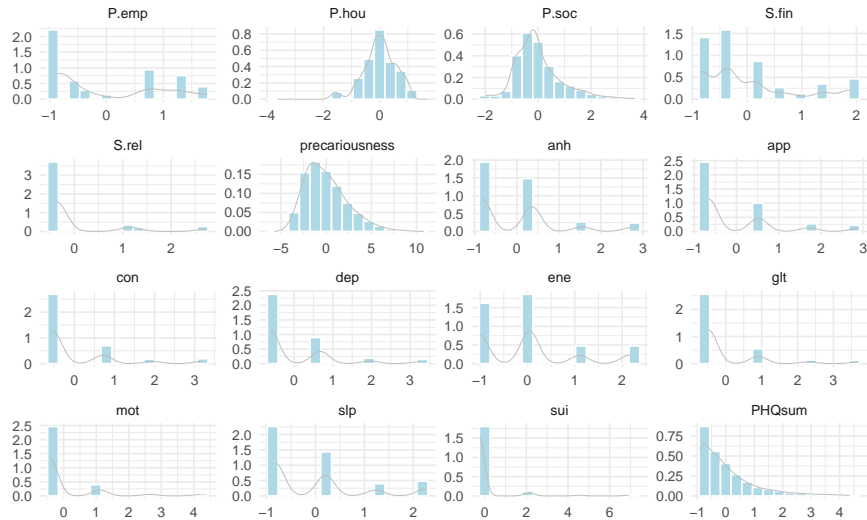


Figure 1: Distributions of variables with density overlay. This shows the distributions of the variables used in the causal analysis, plotted as histograms with overlaid density estimates. The x-axis represents the value of each variable after preprocessing. The y-axis shows the corresponding estimated probability density. **P.emp** = employment precariousness; **P.hou** = housing precariousness; **P.soc** = social precariousness; **S.fin** = recent financial stressors; **S.rel** = recent relational stressors; **precariousness** = overall precariousness; **PHQsum** = PHQ-9 sum score; **anh** = anhedonia; **app** = appetite; **con** = concentration; **dep** = depressed mood; **ene** = energy; **glt** = guilty; **mot** = motor; **slp** = sleep; **sui** = suicidal.

2.2 Causal Discovery

To uncover directional relationships between precariousness and depression, we use constraint-based causal discovery algorithms that allow for feedback loops and latent confounding. Specifically, we apply the *Fast Causal Inference* (FCI) and *Cyclic Causal Inference* (CCI) algorithms, both of which can detect cycles and non-acyclic structures (Mooij & Claassen, 2020; Strobl, 2019). For reference, we also include the PC algorithm, one of the most widely used methods for acyclic causal discovery (Spirtes et al., 2001). While our full analysis includes results from three causal discovery algorithms—FCI, CCI, and PC—we focus on FCI in the main text, as it offers a strong balance between flexibility and theoretical soundness. FCI accommodates latent confounding and potential feedback, making it well-suited for the complexity of our data (Mooij & Claassen, 2020). The PC algorithm is included for reference but relies on more restrictive assumptions, such as acyclicity and no unmeasured confounding. CCI, while capable of modeling cycles explicitly, has its own theoretical limitations; for example, its output may not fully preserve the d-separation properties of the true causal graph (Strobl, 2019). Results from both PC and CCI are provided in the [Appendix](#) (Section 6.4, Section 6.5) for completeness and comparison. For readers interested in detailed explanations of the algorithms, edge interpretations, and graph types (e.g., PAG, MAAG, CPDAG), as well as algorithmic assumptions and limitations, please refer to the [Appendix](#) (Section 6.2).

A key challenge in applying these algorithms to the HELIUS dataset is that many variables are non-Gaussian and likely exhibit nonlinear relationships. While kernel-based conditional independence tests (such as KCIT) are well-suited for capturing such complex dependencies, they are computationally intensive—scaling quadratically with sample size due to the need to invert large kernel matrices—making them impractical for large datasets like HELIUS (Rahimi & Recht, 2007). To address this, we use the Randomized Conditional Correlation Test (RCoT), a nonparametric alternative that approximates kernel methods using random Fourier features. This reduces computational complexity from quadratic to linear in sample size, substantially lowering runtime while preserving sensitivity to nonlinear relationships (Strobl et al., 2019; Zhang et al., 2012). For further details, see Section 6.6.

We examine the causal structure using three complementary approaches:

1. Aggregate-level analysis: relationships between five domain-specific precariousness factors and the PHQ-9 sum score.
2. Fully disaggregated analysis: relationships between individual precariousness items and individual depressive symptoms.
3. Mixed analysis: relationships between individual symptoms and a composite index of overall precariousness.

The aggregate analysis reduces dimensionality and yields interpretable summaries of how domains of precariousness relate to overall depression severity. However, it may obscure finer-grained effects. The disaggregated analysis allows for precise mapping of which symptoms are influenced by (or influence) specific precariousness conditions, but it introduces complexity due to the high dimensionality

and distributional properties of the data. The mixed approach, in turn, integrates these perspectives by examining how individual symptoms respond to cumulative precariousness across domains.

To robustly estimate the causal structure between depression and precariousness variables, we implement a comprehensive bootstrapped causal discovery procedure. This procedure systematically varies key analysis parameters across a grid of configurations, enabling us to assess the stability of inferred relationships under different settings. Specifically, we vary four main components:

- Significance levels for conditional independence tests: $\alpha = 0.01$ and 0.05 .
- Stability thresholds: 0.5 , 0.6 , 0.7 , and 0.8 , which determine how frequently an edge must appear across bootstraps to be retained.
- Conditional independence (CI) tests: Gaussian CI test (partial correlation) and RCoT (a nonparametric test).
- Causal discovery algorithms: FCI, CCI, and PC.

For each unique parameter combination (2 significance levels \times 4 thresholds \times 2 CI tests = 16 settings), we run 100 bootstrap samples per algorithm for the aggregated analyses (see Step 1 in Figure 2). For symptom-level analyses, which are more computationally intensive, we use 30 bootstrap samples per setting.¹

To summarize these results, we apply a two-level aggregation strategy:

1. **Within each condition** (fixed α , threshold, CI test, and algorithm), we identify the most frequently occurring edge type (e.g., arrowhead, circle, none) across bootstraps for each pair of variables (Step 2 in Figure 2).
2. **Across conditions**, we then determine the most dominant edge type based on its frequency. In cases where no edge type is clearly dominant (i.e., a tie), we mark the edge as uncertain, represented with a dashed line in the final graph (Step 3 in Figure 2).

This summarization process is repeated separately for each causal discovery algorithm (FCI, CCI, PC), yielding a single robust graph per algorithm. These final graphs represent only the most stable and consistent relationships across a wide range of plausible parameterizations, enhancing both reliability and interpretability. To support transparency, each final graph is accompanied by a matrix summarizing the relative frequency of each edge type for every variable pair, enabling readers to assess the degree of uncertainty or agreement underlying each connection.

2.3 Modeling Dynamics between precariousness and Depression

To explore how internal system structure shapes responses to external support, we implement a high-level computational model that formalizes key mechanisms suggested by the causal discovery analysis. Rather than attempting to replicate

¹For symptom-level analyses, we further improve computational efficiency by fixing the skeleton structure—the undirected network of potential connections—using a consensus graph derived from all three algorithms (with $\alpha = 0.01$ and the RCoT test). This allows subsequent analyses to focus exclusively on estimating edge directions, avoiding the repeated and costly computation of skeletons, and thus substantially reducing runtime.

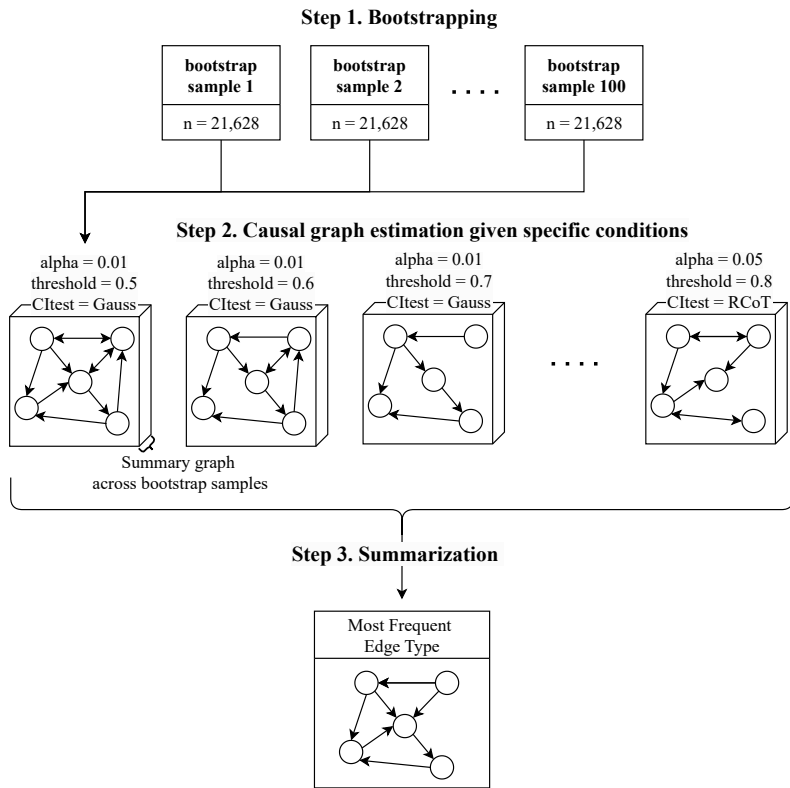


Figure 2: Causal discovery workflow applied across all three algorithms (FCI, CCI, and PC). The process involves three main steps: (1) bootstrapping the dataset to create multiple resampled datasets; (2) estimating causal graphs under varying parameter configurations; and (3) summarizing results by identifying the most frequent edge type across bootstraps and settings to construct a final stable graph.

the full estimated causal graph, this model abstracts the essential structure into a compact, tractable system focused on dynamic interactions between depression and social precariousness, both influenced by financial stress.

As illustrated in Figure 3, the model includes three components: social precariousness $P_i(t)$, depressive symptoms $D_i(t)$, and a static individual-specific external stressor S_i , representing financial stress. Depression and precariousness are modeled as coupled state variables that influence each other over time, with S_i acting as a shared input. These dynamics are formalized as a pair of linear stochastic differential equations (SDEs):

$$\begin{aligned} dP_i(t) &= \lambda_P (\alpha_{PS} S_i + \alpha_{PD} D_i(t) - P_i(t)) dt + \sigma_P dW_{P,i}(t) \\ dD_i(t) &= \lambda_D (\alpha_{DS} S_i + \alpha_{DP} P_i(t) - D_i(t)) dt + \sigma_D dW_{D,i}(t) \end{aligned}$$

Here, $D_i(t)$ denotes the depressive state and $P_i(t)$ denotes the level of social precariousness for individual i at time t , with S_i representing a static, individual-specific external stressor (financial stress). The parameters λ_D , λ_P , as well as the coefficients α and noise terms σ , are assumed to be constant across individuals and time. The parameters λ_D and λ_P govern the timescales over which $D_i(t)$ and $P_i(t)$ adjust toward their respective input-driven target states. The coefficients α_{DS} and α_{PS} quantify the direct effects of the external stressor S_i on depression and precariousness, respectively, while α_{DP} and α_{PD} capture the mutual influence between the two dynamic processes. Stochastic fluctuations are introduced via the independent Wiener processes $dW_{D,i}(t)$ and $dW_{P,i}(t)$, scaled by their respective volatility parameters σ_D and σ_P . This linear structure offers a transparent and analytically tractable framework for modeling how exogenous variation in financial stress may propagate through individual dynamics of depression and precariousness. Crucially, all parameters can be calibrated directly from empirical covariances and variances observed in the HELIUS cohort. The resulting steady-state distribution of the model aligns with empirical measures: PHQ-9 total score (PHQsum) for depression, and the derived social precariousness factor (P.soc) for social precarity. The full calibration procedure is described in Section 2.3.1.

2.3.1 Model Calibration

In our linear model, all parameters are derived analytically to reproduce the empirical second-order moments observed in the HELIUS dataset. The system treats depression (D) and social precariousness (P) as jointly evolving under the influence of a shared external stressor (S), forming a coupled system of Ornstein–Uhlenbeck processes. Under the assumption of stationarity, the steady-state covariances between these variables admit closed-form solutions for the system’s structural parameters.

We fix the adjustment rates $\lambda_D = \lambda_P = 1$, which normalizes the time scale given the cross-sectional nature of the HELIUS data. To resolve the remaining degree of freedom, we treat the feedback from precariousness to depression (α_{DP}) as a free parameter, and we solve algebraically for all other coefficients — specifically the direct effects of stress (α_{DS}, α_{PS}), the reverse feedback from depression to

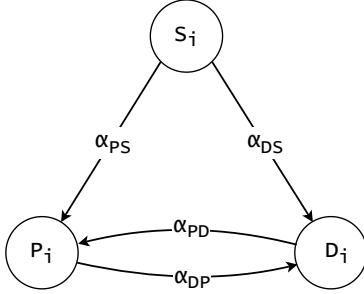


Figure 3: High-level schematic of the dynamic model structure used in simulation. Arrows represent influence coefficients α , matching the terms in the system of stochastic differential equations. $D_i(t)$ and $P_i(t)$ denote depressive symptoms and social precariousness for individual i , with S_i representing static financial stress.

precariousness (α_{PD}), and the noise terms (σ_D, σ_P). These solutions are expressed as closed-form functions of the empirical covariances: $\text{Var}(D)$, $\text{Var}(P)$, $\text{Var}(S)$, $\text{Cov}(D, P)$, $\text{Cov}(D, S)$, and $\text{Cov}(P, S)$.

This structure creates a family of analytically calibrated models, each consistent with the same observed covariances but differing in their internal configuration. We constrain the space of valid solutions by imposing that all structural parameters must be positive, reflecting the assumption that stress and precariousness contribute adversely to depression. This constraint restricts the allowable range of α_{DP} to approximately $[0, 0.698]$ (see Appendix Section 6.7).

Figure 4 illustrates how the remaining parameters adjust as α_{DP} increases to maintain consistency with the empirical covariances. As α_{DP} increases, α_{PD} tends to decrease, reflecting a compensatory trade-off between the mutual influences of depression and precariousness. This interplay helps preserve the model's match with observed covariances, without requiring major shifts in external input strength. Meanwhile, the external coupling terms — α_{DS} and α_{PS} — also shift to absorb variance in a way that maintains alignment with the empirical data. Notably, the noise amplitudes σ_D and σ_P decline slightly as α_{DP} increases. This indicates that more of the observed variability is captured by deterministic interactions, with less left to be explained by stochastic fluctuations.

Rather than being a limitation, this flexibility enables exploration of a spectrum of equally data-consistent feedback regimes. Each represents a different plausible causal architecture, offering insight into how internal dynamics modulate the system's responsiveness to external stress — even when the observed covariances remain unchanged.

2.3.2 Intervention Simulation

To evaluate how internal structure affects system responsiveness, we simulate a family of linear models subjected to external intervention. Each model corresponds

Parameter trade-offs as a function of α_{DP}

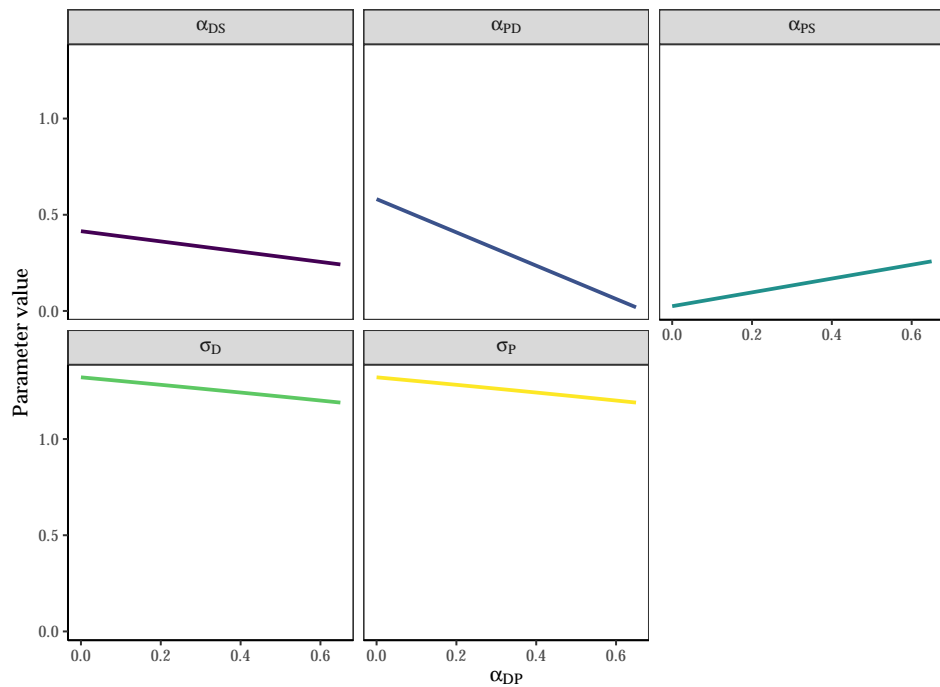


Figure 4: Trade-off curves showing how calibrated parameters vary with α_{DP} . Each line shows how a different parameter adjusts in response to changes in α_{DP} to maintain consistency with empirical covariances from the HELIUS data. All configurations shown are equally consistent with the data, illustrating how internal dynamics adjust as feedback strength changes.

to a different value of α_{DP} , representing the strength of influence from social precariousness to depression. The range spans from 0 (no coupling) to 0.65 (maximal admissible value), with all other parameters derived analytically to preserve the empirical covariances observed in the HELIUS data (see Figure 4).

In each simulation, financial stress of individual i (S_i) is proportionally reduced toward the lowest observed value, modeling a population-wide intervention applied at varying intensities (0–100%). For each model, we simulate 1000 virtual individuals whose baseline stress levels are sampled from the empirical distribution and scaled according to the intervention level.

We assess the system’s behavior using two complementary approaches:

- Snapshot analysis captures the average levels of depression (D) and precariousness (P) at selected time points ($t = 100, 300, 500$) following intervention onset. Since all linear models converge to the same equilibrium, this highlights how internal feedback affects the speed and pathway of adjustment.
- Full trajectory simulation tracks system dynamics over time for two representative models: one with minimal ($\alpha_{DP} = 0$) and one with maximal ($\alpha_{DP} = 0.65$) feedback. Each simulation includes an intervention period followed by its withdrawal, revealing differences in reactivity, delay, and recovery stability.

Together, these simulations demonstrate how internal structure governs not just whether change occurs, but how it unfolds — shaping the pace, persistence, and variability of response to external support.

3 Results

3.1 Causal Structure Linking Precariousness and Depression

3.1.1 Depression as sum score

Figure 5 provides a high-level summary of how precariousness factors collectively influence and are influenced by overall depression severity, focusing on the causal relationships between precariousness factors ($P.hou, P.emp, P.soc, S.rel, S.fin$) and the depression sum score ($PHQsum$), as identified by the FCI algorithm.

In panel (a) we see that employment precariousness ($P.emp$) and social precariousness ($P.soc$) are not identified as causes of depression, whereas financial stress ($S.fin$) appears to play a causal role. While $P.emp$ and $P.soc$ are generally not recognized as causes of other precariousness factors, $S.fin$ emerges as a potential cause, as indicated by its circle edge endpoint. This pattern is further supported by the edge-type proportion matrix shown in panel (b), which aggregates edge inference outcomes across bootstrapped datasets.

Relational stress ($S.rel$) plays a more nuanced role, interacting with depression and $S.fin$ through a latent confounder. Its connection to $P.soc$ is less definitive—the proportion matrix in Figure 5b suggests that this relationship is frequently absent,

ambiguous, or potentially bidirectional across bootstrap samples. Meanwhile, housing precariousness ($P.hou$) is not directly causally related to depression but is linked to $P.emp$ and $S.fin$. While $P.emp$ and $S.fin$ are identified as non-causes of $P.hou$, it remains unclear whether $P.hou$ causally influences $P.emp$ or if their relationship is mediated by an unobserved confounder.

The findings from the CCI algorithm (see Figure 10) are largely consistent with those from the FCI analysis, with one key distinction: CCI shows greater ambiguity in the directional relationship between $S.fin$ and $PHQsum$: CCI assigns an arrowhead from $S.fin$ to $PHQsum$ in roughly 50% of bootstraps, while the remaining cases display an undirected (circle) endpoint. Overall, CCI introduces greater uncertainty in edge orientations relative to FCI, yielding more undirected endpoints and more frequent bidirectional (confounded) edges, which in turn contribute to a slightly higher overall count of arrowheads when directions are inferred. Both algorithms identify directional pathways from the stressors ($S.rel$, $S.fin$) to $P.soc$ and suggest that $P.soc$ is not a cause of $PHQsum$, but more likely affected by it. $P.emp$ is not inferred to cause any of its neighboring variables ($P.hou$, $PHQsum$, $S.fin$) and instead appears to be affected by them. $P.hou$, in turn, is connected to $P.emp$ and $S.fin$ with circle endpoints, indicating that it may be a potential source of influence rather than an outcome.

Causal relationships between five precariousness factors and depression sum score ($PHQsum$), as estimated using the FCI algorithm across bootstrapped samples. (a) Aggregated causal graph showing the most frequent edge types across bootstraps. Dashed edges indicate ties, with a bold horizontal bar marking where the tie occurs. (b) Proportion matrix summarizing edge types across all bootstraps. Each matrix cell $[i, j]$ represents how often an edge from variable i to variable j exhibited a particular edge mark—arrowhead, tail, circle, or no edge—adjacent to j . The edge mark in matrix $[i, j]$ reflects the orientation of the edge ending at j . For example, if matrix $[i, j]$ shows a green arrowhead ($>$) and matrix $[j, i]$ shows a blue circle (\circ), then the inferred relationship is $i \rightarrow j$. Edge types are encoded by distinct colors: green for arrowheads, coral for arrowtails, blue for circles, and light gray for absence of an edge. Colors are blended and shaded by frequency, with greater opacity indicating higher confidence in the inferred edge type.

3.1.2 Individual depression symptom

Moving from the sum score representation to the disaggregated symptom-level graph provides a more granular perspective on the causal relationships between precariousness factors and depression symptoms. Unlike the sum score graph, which aggregates all symptoms into a single measure, the symptom-level graph in Figure 6 reveals the heterogeneity in how specific symptoms (*con* (concentration), *slp* (sleep), *ene* (energy), *app* (appetite), *mot* (motor), *sui* (suicidal), *anh* (anhedonia), *glt* (guilt), and *dep* (depressed mood)) are influenced by, and in turn influence, different forms of precariousness.

Figure 6a reveals a strong interdependence among symptoms and suggests much presence of latent confounders, as indicated by numerous bidirectional edges. In Figure 6b, the proportion matrix indicates that arrowheads are the most frequently

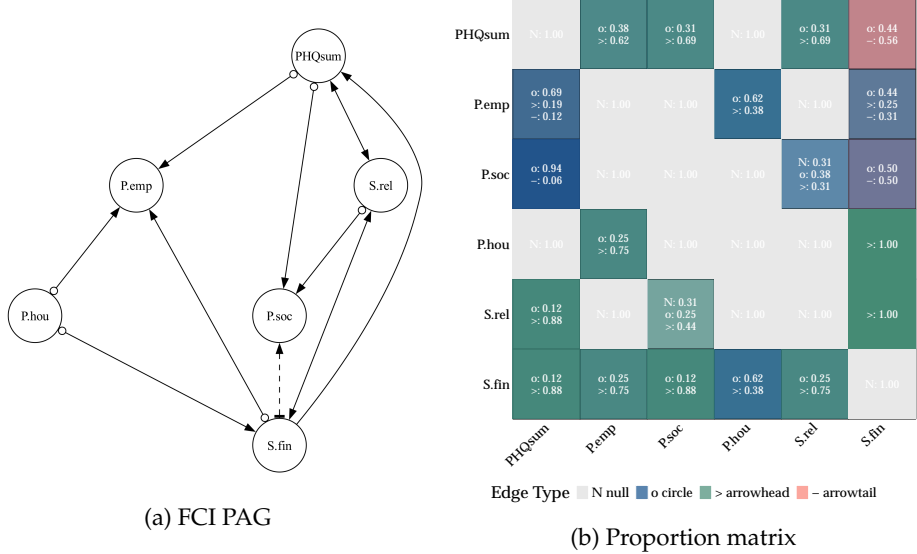


Figure 5: Causal relationships between five precariousness factors and depression sum score ($PHQsum$), as estimated using the FCI algorithm across bootstrapped samples. **(a)** Aggregated causal graph showing the most frequent edge types across bootstraps. Dashed edges indicate ties, with a bold horizontal bar marking where the tie occurs. **(b)** Proportion matrix summarizing edge types across all bootstraps: each matrix cell $[i, j]$ indicates how often a given edge from variable i to variable j exhibited a particular edge mark (e.g., arrowhead, tail, or circle) adjacent to j . Green indicates arrowheads, coral arrowtails, blue circle marks, and gray absence of an edge. Colors are blended and shaded by frequency, with dominant symbols appearing more opaque. For example, matrix $[S.fin, PHQsum]$ shows a green arrowhead ($>$) and matrix $[PHQsum, S.fin]$ shows a coral arrowtail ($-$), together indicating that $S.fin \rightarrow PHQsum$ in the majority of bootstrapped graphs.

inferred edge type. However, circle endpoints are particularly common for *anh*, *slp*, *ene*, and *sui*, reflecting uncertainty in the causal direction among these symptoms. Notably, the only arrowtail connection appears between *dep* and *anh*, suggesting that anhedonia is a potential cause of depressed mood.

Looking at the symptom-precariousness connections, one of the key patterns is that ties are most frequently found in the relationships between individual symptoms and precariousness factors. This suggests that these causal links may be less stable across different conditions. Closer examination reveals that most ties arise due to discrepancies between the Gaussian CI test and the RCoT test—with Gaussian CI favoring arrowheads and RCoT more often predicting the absence of an edge.

Despite these differences, some consistent patterns emerge across both CI tests, particularly in the case of *S.fin*, which appears to be connected to nearly all other variables—though many of these connections are marked by ties, reflecting uncertainty in directionality. One exception is the stronger evidence suggesting that *S.fin* may cause changes in *app*, while its relationships with other symptoms, such as *ene*, *mot*, and *dep*, remain ambiguous. Similarly, *P.soc* exhibits numerous connections with depressive symptoms, with most edges pointing toward *P.soc* rather than outward from it. This suggests that depressive symptoms, particularly *dep* and *glt*, may contribute to worsening social precariousness rather than the other way around. Additionally, *anh* also shows signs of a potential causal influence on *P.soc*, reinforcing the idea that social precariousness is more often a consequence rather than a driver of depressive symptoms.

Other precariousness factors exhibit more uncertainty but still notable relationships. *S.rel* is connected to *slp*, *glt*, and *app*, though directionality remains unclear in many cases. *P.emp* also connects to symptoms like *slp*, *mot*, and *con*, but, like *S.rel*, these relationships exhibit a 50/50 split in directionality, reflecting uncertainty in the inferred causal paths. In line with the aggregated graph in Figure 5, *P.hou* does not appear to have any direct relationship with depression symptoms but consistently shows associations with *P.emp* and *S.fin*. The causal relationships among precariousness factors remain largely unchanged from the aggregated analysis, with *S.fin* exhibiting the strongest tendency to influence other precariousness factors.

Among depressive symptoms, *dep*, *glt*, and *slp* appear to be the most connected to precariousness factors, while *P.soc* has the most connections with symptoms, predominantly as a recipient rather than a driver of influence. Within the symptom network, *slp*, *sui*, and *anh* emerge as causally influential symptoms, as they exhibit more outgoing arrows compared to other symptoms. On the other hand, *con*, *mot*, *dep*, and *glt*, despite having high connectivity, predominantly receive incoming arrows, indicating they are more likely effects rather than causes. Considering both symptom-precariousness connections and symptom-level dynamics, *slp* emerges as a central symptom, given its strong ties to precariousness factors and its influential role within the symptom network. *P.soc* appears to function as a bridge between the depression and precariousness subsystems, as depressive symptoms appear to feed back into social precariousness, reinforcing a self-sustaining dynamic between depression and precarious conditions.

Finally, the results from CCI are largely consistent with those from FCI, but with some key differences. CCI tends to favor arrowheads more frequently, resulting in a greater number of bidirectional edges, which suggests a higher involvement of latent confounders. Additionally, CCI exhibits more tie situations, though, similar to FCI, most ties occur between absence and arrowhead edges, reflecting the discrepancy between the Gaussian CI test and RCoT—where the Gaussian test favors arrowheads, while RCoT more often suggests the absence of an edge. For a detailed visualization of the CCI-derived graph and proportion matrix, see Figure 11.

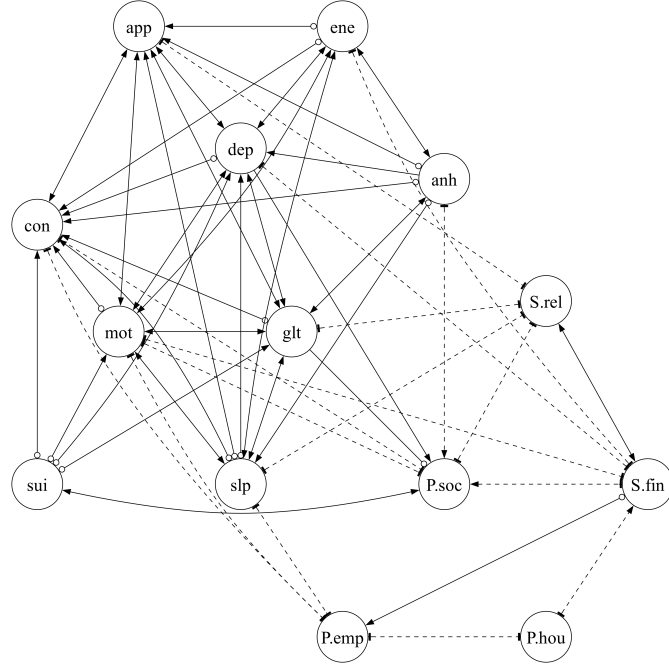
3.1.3 Precariousness as sum score

Lastly, we examine the relationships between individual symptoms and overall precariousness, an aggregated measure represented by the sum of five precariousness factors. This analysis provides a complementary perspective, capturing broader patterns that may not be evident in the disaggregated symptom-precariousness analysis. By aggregating precariousness factors into a single score, this approach may capture distributed relationships across different precariousness factors that were previously overlooked in the disaggregated analysis.

Unlike the disaggregated graph in Figure 6, the aggregated symptom-precariousness graph (Figure 7a) shows greater certainty in causal directions, with ties occurring only in edges involving the overall precariousness factor. This is even more evident in the proportion matrix (Figure 7b), where symptom-to-symptom interactions almost fully converge to a single edge type. Additionally, all symptom interactions are connected either through bidirectional edges or a combination of an arrowhead and a circle, suggesting a strong presence of latent confounders.

Examining the symptom-precariousness connections, we observe a stronger overall trend of depressive symptoms influencing precariousness, rather than the other way around. Specifically, *anh*, *dep*, and *slp* frequently emerge as sources of influence on precariousness, whereas *app*, *glt*, and *mot* exhibit more uncertainty in directionality, often resulting in circle endpoints. This pattern suggests that when precariousness factors are aggregated, the dominant causal flow is from depressive symptoms to precariousness, rather than precariousness driving depression. Particularly, *dep* emerges as the strongest predictor of precariousness, exhibiting the highest proportion of arrowtails, consistent with findings from the disaggregated analysis.

Comparing this with the CCI-derived graph (Figure 12), several key differences stand out. The CCI results reveal that most symptoms are interconnected through bidirectional edges, suggesting a strong presence of latent confounders. However, *dep* appears to be a distinct exception, as it is predominantly caused by nearly all other symptoms, with one exception *sui*, which does not contribute to *dep*. Similarly, *con* is influenced by multiple symptoms, albeit with weaker support compared to *dep*. Most interestingly, the CCI results highlight a distinct feedback loop between *dep* and overall precariousness, represented by a tail-tail edge (—). This suggests a possible reinforcing cycle between depression and overall precariousness, where



(a) FCI PAG

	anh	> 1.00	> 1.00	> 1.00	> 1.00	> 1.00	> 1.00	> 1.00	N: 1.00	N: 1.00	N: 1.00	N: 1.00	N: 1.00	N: 1.00	N: 1.00	N: 1.00	
anh	N: 1.00	> 1.00	> 1.00	> 1.00	> 1.00	> 1.00	> 1.00	> 1.00	N: 1.00	N: 1.00	N: 1.00	N: 1.00	N: 1.00	N: 1.00	N: 1.00	N: 1.00	
dep	o: 0.12 -: 0.88	N: 1.00	o: 0.75 -: 0.25	o: 0.12 -: 0.88	o: 0.38 -: 0.62	o: 0.25 -: 0.50	o: 0.12 -: 0.88	o: 0.38 -: 0.62	o: 0.62 -: 0.38	N: 0.50 -: > 0.50	N: 0.38 -: > 0.50	N: 1.00					
slp	N: 1.00	> 1.00	N: 1.00	o: 0.38 -: > 0.62	o: 0.25 -: > 0.75	> 1.00	> 1.00	> 1.00	N: 1.00	N: 1.00	N: 1.00	N: 1.00	N: 1.00	N: 1.00	N: 1.00	N: 1.00	
ene	> 1.00	> 1.00	> 1.00	N: 1.00	> 1.00	N: 1.00	> 1.00	> 1.00	N: 1.00	N: 1.00	N: 1.00	N: 1.00	N: 1.00	N: 1.00	N: 1.00	N: 1.00	
app	o: 0.62 -: 0.38	> 1.00	o: 0.62 -: > 0.38	o: 0.62 -: > 0.38	N: 1.00	> 1.00	> 1.00	> 1.00	N: 1.00	N: 1.00	N: 1.00	N: 1.00	N: 1.00	N: 1.00	N: 1.00	N: 1.00	
glt	> 1.00	> 1.00	> 1.00	N: 1.00	> 1.00	N: 1.00	> 1.00	> 1.00	o: 0.25 -: > 0.75	N: 1.00	o: 0.25 -: > 0.75	N: 1.00					
con	o: 0.62 -: 0.38	o: 0.25 -: > 0.75	o: 0.75 -: > 0.25	o: 0.62 -: > 0.38	o: 0.62 -: > 0.38	o: 0.12 -: > 0.50	o: 0.75 -: > 0.25	o: 0.62 -: > 0.38	o: 0.62 -: > 0.38	N: 0.50 -: > 0.50	N: 0.50 -: > 0.50	N: 1.00					
mot	N: 1.00	> 1.00	> 1.00	> 1.00	> 1.00	> 1.00	> 1.00	> 1.00	N: 1.00	N: 1.00	N: 1.00	N: 1.00	N: 1.00	N: 1.00	N: 1.00	N: 1.00	
sui	N: 1.00	> 1.00	N: 1.00	N: 1.00	N: 1.00	> 1.00	> 1.00	> 1.00	N: 1.00	N: 1.00	N: 1.00	N: 1.00	N: 1.00	N: 1.00	N: 1.00	N: 1.00	
P.emp	N: 1.00	N: 0.50 o: 0.38 -: > 0.12	N: 0.50 o: 0.12 -: > 0.50	N: 1.00	N: 0.50 o: 0.25 -: > 0.50	N: 1.00	N: 0.88 o: 0.12 -: > 0.12	N: 1.00									
Psoc	N: 1.00	N: 0.38 o: 0.12 -: > 0.50	N: 1.00	N: 0.50 o: 0.25 -: > 0.50	N: 1.00	N: 0.88 o: 0.12 -: > 0.12	N: 1.00										
P.hou	N: 0.50 o: 0.25 -: > 0.25	N: 1.00	N: 1.00	N: 1.00	N: 0.75 o: 0.25 -: > 0.25	N: 1.00	N: 1.00	N: 1.00	N: 1.00	N: 0.50 o: 0.12 -: > 0.50	N: 1.00	N: 1.00	N: 1.00	N: 1.00	N: 1.00	N: 1.00	
S.rel	N: 1.00	N: 1.00	N: 0.50 o: 0.50 -: > 0.50	N: 1.00	N: 0.50 o: 0.50 -: > 0.50	N: 1.00	N: 1.00	N: 1.00	N: 0.50 o: 0.50 -: > 0.50	N: 1.00	N: 0.50 o: 0.12 -: > 0.50	N: 1.00					
S.fin	N: 0.50 o: 0.38 -: > 0.12	N: 0.50 o: 0.50 -: > 0.50	N: 0.88 o: 0.50 -: > 0.12	N: 0.50 o: 0.50 -: > 0.50	N: 1.00	N: 0.38 o: 0.25 -: > 0.38	N: 1.00										

Edge Type ■ N null ■ o circle ■ > arrowhead ■ - arrowtail

(b) Proportion matrix

Figure 6: Resulting graph of precariousness factors and individual depression symptoms using FCI and proportion of edge endpoint types.

depression not only arises from precarious conditions but also contributes to their persistence, creating a self-sustaining dynamic.

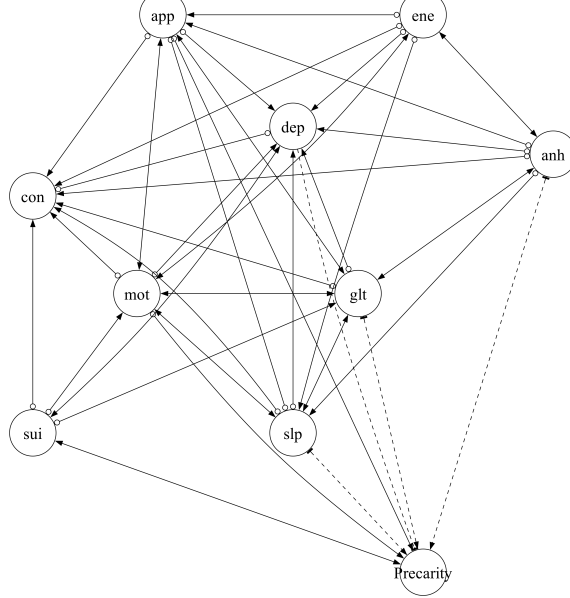
Across multiple levels of analysis, our results point to a consistent and directional link between precariousness and depression. Financial stress ($S.fin$) emerges as a particularly robust and modifiable upstream driver: in both aggregated and disaggregated models, it shows strong and stable causal influence on depressive symptoms. By contrast, other forms of precariousness—particularly social precarity—more often appear as outcomes rather than antecedents of depression, frequently receiving rather than sending causal arrows. Among symptoms, dep and slp stand out for their centrality and connections to precariousness factors, with dep also implicated in potential feedback loops with social precarity ($P.soc$). These findings motivate the use of a simplified three-node model in the simulation—capturing depression, financial stress, and social precarity—as it preserves the key dynamic motifs observed in the causal graphs while enabling tractable exploration of system-level responses to stress-reducing interventions.

3.2 Simulating the Dynamics Between Precariousness and Depression Under Intervention

To assess how internal structure influences the system’s responsiveness to external support, we simulate a set of linear models that are consistent with the data but vary in the assumed strength of influence from precariousness to depression (α_{DP}). For each model, we generate a virtual population of 1,000 individuals and simulate an external intervention that reduces each individual’s financial stress (S) proportionally toward the minimum observed value in the dataset. While individuals begin with different baseline stress levels, the intervention applies a shared proportional reduction across the population. This intervention defines the external input, while variation in α_{DP} reflects different assumptions about internal feedback from precariousness to depression. We examine system behavior in two complementary ways: (1) by analyzing average levels of depression and precariousness at selected time points following intervention onset, and (2) by simulating full temporal trajectories under sustained intervention followed by recovery, using two representative cases at the extremes of the α_{DP} range.

Figure 8 summarizes how variation in α_{DP} shapes system-level responses to external support. In Panel A, during the early phase of intervention, depression and precariousness exhibit contrasting patterns. Depression declines more rapidly in scenarios with lower α_{DP} , where its dynamics are driven more directly by the external stressor S . As α_{DP} increases, D becomes more dependent on precariousness (P), which itself adjusts more slowly—delaying the depressive response. Precariousness, by contrast, shows slightly faster early reductions in scenarios with higher α_{DP} . This reflects a shift in influence: as α_{DP} increases, P becomes more directly responsive to S (via increasing α_{PS}) and less influenced by D , allowing it to adjust more promptly to changes in the stressor.

Despite these short-term differences, all scenarios ultimately converge to similar steady-state levels under sustained intervention. AS the systm approaches conver-



(a) FCI PAG

	anh	>: 1.00	>: 1.00	>: 1.00	>: 1.00	>: 1.00	>: 1.00	>: 1.00	>: 1.00	>: 1.00
anh	N: 1.00									
dep	<: 1.00	N: 1.00		<: 1.00	<: 1.00	<: 0.62 >: 0.38	<: 1.00	<: 0.88 >: 0.12	<: 0.38 >: 0.62	<: 0.50 >: 0.50
sui										
slp	<: 1.00	>: 1.00	N: 1.00	<: 1.00	<: 1.00	>: 1.00	>: 1.00	>: 1.00	N: 1.00	>: 1.00
ene	>: 1.00	>: 1.00	>: 1.00	N: 1.00	>: 1.00	N: 1.00	>: 1.00	>: 1.00	N: 1.00	N: 1.00
app	<: 1.00	>: 1.00	<: 1.00	<: 1.00	N: 1.00	>: 1.00	>: 1.00	>: 1.00	N: 1.00	>: 1.00
glt	>: 1.00	>: 1.00	>: 1.00	N: 1.00	>: 1.00	N: 1.00	>: 1.00	>: 1.00	<: 1.00	>: 1.00
con	<: 1.00	<: 1.00	<: 0.88 >: 0.12	<: 1.00	<: 1.00	<: 1.00	N: 1.00	<: 0.88 >: 0.12	<: 0.62 >: 0.38	N: 0.62 >: 0.38
mot	N: 1.00									
sui	N: 1.00	>: 1.00	N: 1.00	N: 1.00	N: 1.00	>: 1.00	>: 1.00	>: 1.00	N: 1.00	>: 1.00
precarity	<: 0.50 -: 0.50	<: 0.38 -: 0.50	<: 0.50 -: 0.50	N: 1.00	<: 0.62 -: 0.38	<: 0.50 -: 0.50	N: 0.62 -: 0.38	<: 0.88 -: 0.12	<: 0.12 -: 0.88	N: 1.00

Edge Type ■ N null ■ o circle ■ > arrowhead ■ - arrowtail

(b) Proportion matrix

Figure 7: Resulting graph of precariousness sum score and individual depression symptoms using FCI and proportion of edge endpoint types. As before, dashed edges denote ties, with specific ties marked by bold horizontal bars.

gence, some variation remains, particularly in P , where gradients between models are still visible. This convergence highlights that the key distinctions lie not in whether intervention is effective, but in how quickly and through which pathways change unfolds.

Panel B shows full time trajectories for two representative cases: one with minimal internal feedback ($\alpha_{DP} = 0$) and one at the upper admissible limit ($\alpha_{DP} = 0.65$). In both, there is a temporary intervention period. When $\alpha_{DP} = 0$, depression responds rapidly to the reduction in stress and rebounds shortly after support is withdrawn. In contrast, when α_{DP} is high, D responds more gradually and recovers more slowly—reflecting its increased dependence on the slower-changing P . Precariousness declines in both scenarios during intervention and returns to baseline afterward, but with a slightly sharper drop in the higher α_{DP} condition. This occurs because P becomes more directly responsive to S , as consistency with the data requires α_{PS} to increase with α_{DP} (see Figure 4). These parameter shifts reflect trade-offs needed to preserve the empirical covariances, with further details provided in Appendix Section 6.7.

These asymmetries further highlight how internal structure—not just external inputs—shapes the system’s trajectory. Specifically, changes in coupling parameters reconfigure how stress reduction propagates through the system, altering the speed and pathway of response even when long-run outcomes remain unchanged.

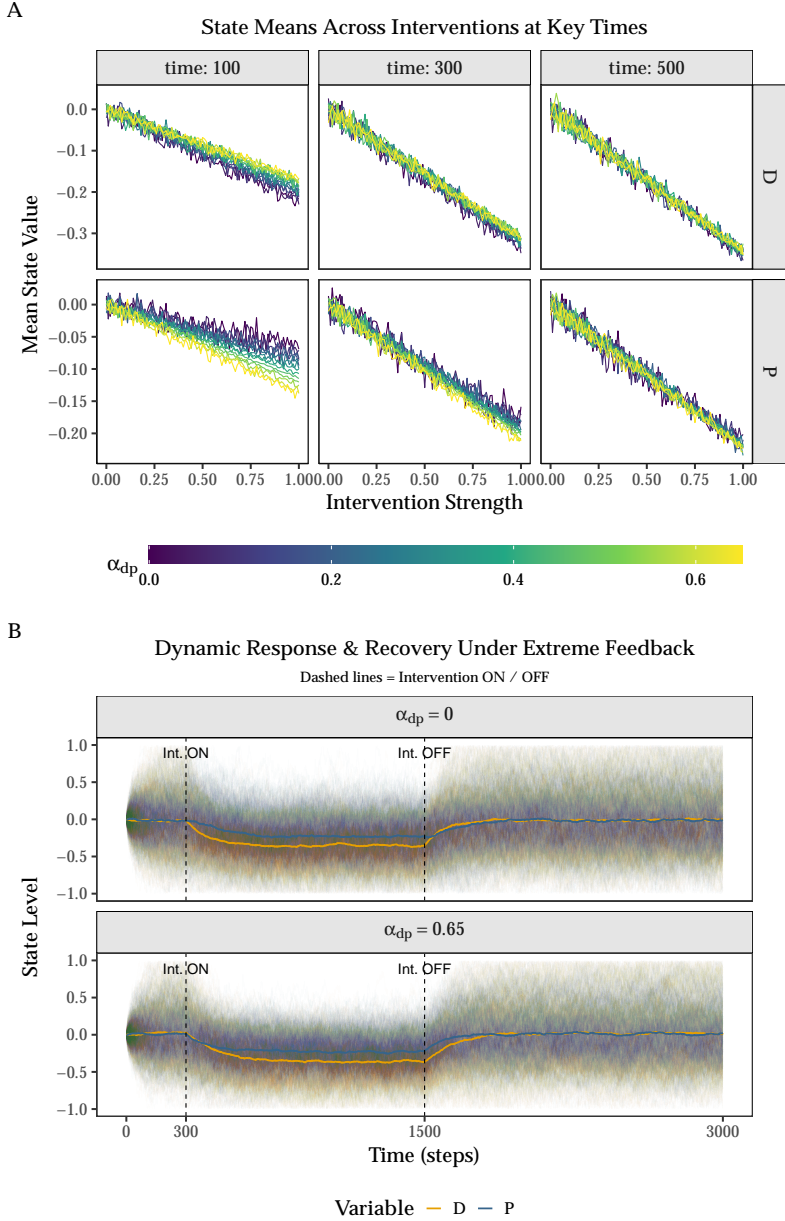


Figure 8: System response to external intervention across variations in internal structure. **Panel A:** Mean levels of depression (D) and precariousness (P) at time steps 100, 300, and 500, across varying values of α_{DP} and intervention strengths. The x-axis represents the strength of external support, operationalized as the proportional reduction of financial stress (S) toward its minimum observed value. Each line corresponds to a different model defined by a specific α_{DP} value, color-coded from low (purple) to high (yellow). Models with lower α_{DP} exhibit faster early reductions in D , while higher α_{DP} leads to more immediate declines in P . **Panel B:** Full time trajectories for two models—one with no coupling ($\alpha_{DP} = 0$) and one with strong coupling ($\alpha_{DP} = 0.65$)—illustrating system response and recovery following intervention onset (step 300) and withdrawal (step 1500). Depression responds more gradually and persistently in the high α_{DP} model, whereas precariousness adjusts more quickly.

4 Discussion

This study combined constraint-based causal discovery and dynamical modeling to investigate how depression and socioeconomic precariousness interact and how their internal structure modulates responsiveness to intervention. Consistent with prior work linking financial strain to psychological distress (Ezzy, 1993; Lund et al., 2010), our analysis identified financial stress as a key upstream driver of depression in both aggregated and disaggregated models. This supports longstanding hypotheses that economic stressors can act as modifiable entry points into broader cycles of psychosocial risk.

At the symptom level, our analysis aligns with established theories of psychopathology but provides a more fine-grained map of potential causal relationships, generating concrete, testable hypotheses. It also points to possible limitations of prevailing models, as some observed symptom–symptom links may be shaped by shared confounders rather than direct causal influence. This suggests that, in some contexts, broader mechanisms or clusters of symptoms may provide more effective units of analysis and intervention than individual symptoms alone. Within this framework, sleep disturbance emerged as a potentially initiating symptom, with directed connections to both symptom-level and precariousness variables—mirroring longitudinal findings that identify sleep disruption as an early warning signal for depressive episodes and social withdrawal (Alvaro et al., 2013; Zawadzki et al., 2013). Depressed mood, another core symptom, occupied a central position in the network. Not only was it influenced by upstream symptoms like anhedonia and guilt, but it also showed directional influence on social precariousness—suggesting that internal psychological states may actively shape external vulnerability. The CCI algorithm further identified a potential feedback loop between depressed mood and overall precariousness, resonating with social drift theories in depression, which posit that declining mental health can lead to social exclusion, job instability, and housing insecurity, reinforcing depressive cycles (Boschloo et al., 2015; Compton & Shim, 2015).

In contrast, social precariousness itself appeared more often as an effect than a cause, receiving arrows from symptoms like depressed mood and guilt but rarely sending them. This asymmetry supports prior observations that indicators of social vulnerability often reflect downstream consequences of poor mental health, though the relationships are likely bidirectional over time (Lund et al., 2010). Although our findings are based on Amsterdam-specific data, they align with research in other high-income urban settings, where structural inequalities such as poverty, unemployment, and housing insecurity consistently predict poor psychological outcomes (Fryers et al., 2003; Weich & Lewis, 1998). While local contexts may alter specific pathways, these parallels suggest that similar mechanisms could operate elsewhere, though replication in other populations is needed to assess robustness.

Taken together, these findings yield actionable insights for mental health intervention. Symptoms like sleep disturbance, which demonstrate early and broad influence across both symptom and precariousness networks, may serve as effective targets for prevention—potentially halting the progression into more entrenched depressive states or worsening precariousness. Similarly, targeting symptoms

such as depressed mood, which appear embedded in potential feedback loops linking psychological and social domains, may offer strategic leverage for breaking mutually reinforcing cycles of mental decline and social isolation. Importantly, interventions targeting such nodes may have ripple effects across domains. For instance, evidence suggests that treating core depressive symptoms can improve social functioning, employment engagement, and housing stability—particularly when combined with social or financial supports (Lund et al., 2018; McDaid et al., 2019). These dual benefits underscore the value of integrated, cross-domain strategies that simultaneously address internal symptoms and external stressors.

Our results also highlight why single-point interventions may fail to produce lasting change. The broader causal structure reveals multiple interlocking feedback loops spanning both psychological symptoms and structural risk factors, which may re-amplify vulnerability even after temporary relief. Supporting this, recent simulation work by Park, Li, et al. (2025) shows that feedback loops, even when modest in strength, can substantially diminish the long-term impact of isolated interventions unless multiple reinforcing links are simultaneously disrupted. Our own simulations support this view: while all models converged to similar long-term outcomes under sustained support, differences in internal structure—specifically, the strength of the link from precariousness to depression—produced systematic variation in how quickly and through which pathways systems responded to intervention. Stronger coupling slowed recovery and prolonged depression, showing that internal architecture can be as important as external input. This supports growing calls for systems-oriented mental health perspectives (Borsboom, 2017). Rather than assuming uniform responses, more durable outcomes may require (1) targeting early-acting symptoms, (2) sustaining support where recovery is slow, and (3) combining structural and psychological interventions. Tailoring strategies to match the system’s architecture can improve effectiveness, particularly in populations with layered vulnerabilities. In this light, understanding causal architecture is not merely theoretical—it is foundational to designing more effective and equitable interventions.

While the FCI and CCI algorithms are designed to recover causal structure from cross-sectional data—including feedback and latent confounding—many edge directions in our results remain ambiguous, particularly in links between individual symptoms and precariousness factors. These inconsistencies likely reflect limited statistical signal in high-dimensional settings, where large conditioning sets reduce power and small effect sizes are harder to detect. Moreover, our findings showed sensitivity to the choice of conditional independence (CI) test. The Gaussian CI test, which assumes linearity and Gaussian noise, often produced denser graphs, likely due to overestimating weak or noisy linear associations. In contrast, RCoT, a nonparametric alternative, avoids these assumptions but relies on a Gaussian radial basis function (RBF) kernel to assess dependence. While flexible in capturing nonlinear relationships, this kernel is optimized for smooth, continuous variables and may underperform with discrete or ordinal data. Its similarity estimates can be unreliable when applied to variables with discontinuities, potentially leading to missed dependencies. This is particularly relevant in the HELIUS dataset, where some variables are ordinal or mixed-type (Howlett, 2001). To address this, future

work should consider adapting kernel-based CI tests to better handle mixed data structures—for example, by employing hybrid kernels that explicitly combine continuous and discrete similarity measures. This could improve the reliability of nonparametric causal discovery in settings with heterogeneous variable types.

Although the CCI algorithm is explicitly designed to detect cycles, aside from the connection between precarity and depression in the aggregate precarity setting, we found little clear evidence of feedback: most candidate loops appeared only as bidirectional edges, which may reflect latent confounding or statistical imprecision. This could point to either an absence of strong feedback at the symptom and the precariousness factor levels or limitations in the sensitivity of full-graph discovery approaches applied to densely interconnected variables. More focused strategies, such as local structure tests or theory-guided subgraph modeling, may help resolve these ambiguities. Moreover, our analyses relied solely on observational data from the Amsterdam population. Some structural uncertainties, particularly those involving latent confounding or bidirectional influence, may ultimately require interventional or semi-interventional designs. Extensions such as LLC (Hyttinen et al., 2012), NODAGS-Flow (Sethuraman et al., 2023), or Bicycle (Rohbeck et al., 2024), which integrate observational and interventional data, could be especially valuable where such data are available.

Finally, the structure of our dynamical model introduces important limitations. The model focused on a restricted set of variables (depression, social precariousness, and financial stress). This design was intentionally simplified to isolate core mechanisms of interest, but it necessarily omits other relevant domains of precariousness, additional stressors, and potential unintended consequences of intervention. In addition, while the linear formulation offered analytical tractability and transparent calibration, it likely oversimplifies the true dynamics of depression and socioeconomic precariousness. A growing body of evidence suggests that psychosocial systems are fundamentally nonlinear. Empirical and theoretical work points to phenomena such as threshold effects, where improvements only occur after a tipping point is crossed (Leemput et al., 2014; Park, Waldorp, et al., 2025); saturation, where the impact of support diminishes as basic needs are met (Cramer et al., 2010); and path dependence, where past adversity shapes sensitivity to future stressors (Wichers et al., 2016). These behaviors are fundamentally incompatible with linear dynamics, yet they may be essential for understanding why some individuals remain trapped in high-risk states while others recover more easily. Future modeling efforts should therefore incorporate mechanisms such as saturating input-response functions (e.g., sigmoidal form) and state-dependent feedback (where coupling strength varies by system state). Incorporating such features would allow models to capture not just average effects but also the critical conditions under which meaningful change becomes possible—clarifying whether some subgroups require forceful, threshold-crossing interventions, while others may benefit from sustained, moderate support.

As public health research has long shown, social and psychological systems do not always respond passively to external inputs; internal constraints can limit the impact of even well-intentioned policies (Savigny & Adam, 2009; Wagenaar &

Burris, 2013). By using causal discovery and computational modeling, researchers and policymakers can better identify these structural constraints and tailor interventions accordingly. More broadly, this study offers a generalizable framework for investigating complex mental health dynamics. Causal discovery supports principled hypothesis generation from observational data, while dynamical modeling enables exploration of how hypothesized structures behave under external change. Together, these tools move us beyond static descriptions toward mechanistic insight with direct relevance for real-world mental health policy and intervention design. Future research should build on this foundation by developing richer, more nuanced dynamical models grounded in longitudinal and interventional data. Incorporating time, multiple domains of precarity, and adaptive feedback processes would help assess whether the mechanisms proposed manifest in actual mental health trajectories. Ultimately, we hope this study encourages further integration of causal structure learning and systems modeling in efforts to understand and improve mental health outcomes under conditions of socioeconomic precariousness.

5 References

- Alvaro, P. K., Roberts, R. M., & Harris, J. K. (2013). A systematic review assessing bidirectionality between sleep disturbances, anxiety, and depression. *Sleep*, 36(7), 1059–1068.
- Borsboom, D. (2017). A network theory of mental disorders. *World Psychiatry*, 16(1), 5–13.
- Boschloo, L., Van Borkulo, C. D., Rhemtulla, M., Keyes, K. M., Borsboom, D., & Schoevers, R. A. (2015). The network structure of symptoms of the diagnostic and statistical manual of mental disorders. *PloS One*, 10(9), e0137621.
- Butterworth, P., Olesen, S. C., & Leach, L. S. (2012). The role of hardship in the association between socio-economic position and depression. *Australian & New Zealand Journal of Psychiatry*, 46(4), 364–373.
- Compton, M. T., & Shim, R. S. (2015). The social determinants of mental health. *Focus*, 13(4), 419–425.
- Cramer, A. O., Waldorp, L. J., Van Der Maas, H. L., & Borsboom, D. (2010). Comorbidity: A network perspective. *Behavioral and Brain Sciences*, 33(2-3), 137–150.
- Deb, K., Pratap, A., Agarwal, S., & Meyarivan, T. (2002). A fast and elitist multiobjective genetic algorithm: NSGA-II. *IEEE Transactions on Evolutionary Computation*, 6(2), 182–197.
- Dojer, N. (2016). Learning bayesian networks from datasets joining continuous and discrete variables. *International Journal of Approximate Reasoning*, 78, 116–124.
- Elsenburg, L. K., Nicolaou, M., Galenkamp, H., Lakerveld, J., & Stronks, K. (2025). The clustering of disadvantage in different life dimensions across ethnic groups: A network analysis of indicators of precariousness in the HELIUS study. *Social Science & Medicine*, 117970.
- Entner, D., & Hoyer, P. O. (2010). On causal discovery from time series data using FCI. *Probabilistic Graphical Models*, 16.
- Epskamp, S., Borkulo, C. D. van, Veen, D. C. van der, Servaas, M. N., Isvoraru,

- A.-M., Riese, H., & Cramer, A. O. (2018). Personalized network modeling in psychopathology: The importance of contemporaneous and temporal connections. *Clinical Psychological Science*, 6(3), 416–427.
- Ezzy, D. (1993). Unemployment and mental health: A critical review. *Social Science & Medicine*, 37(1), 41–52.
- Fone, D., White, J., Farewell, D., Kelly, M., John, G., Lloyd, K., Williams, G., & Dunstan, F. (2014). Effect of neighbourhood deprivation and social cohesion on mental health inequality: A multilevel population-based longitudinal study. *Psychological Medicine*, 44(11), 2449–2460.
- Forré, P., & Mooij, J. M. (2018). Constraint-based causal discovery for non-linear structural causal models with cycles and latent confounders. *arXiv Preprint arXiv:1807.03024*.
- Franz, R., & Nakamura, R. (2015). *nsga2R: Elitist non-dominated sorting genetic algorithm for multi-objective optimization*. <https://CRAN.R-project.org/package=nsga2R>
- Fryers, T., Melzer, D., & Jenkins, R. (2003). Social inequalities and the common mental disorders: A systematic review of the evidence. *Social Psychiatry and Psychiatric Epidemiology*, 38(5), 229–237.
- Galenkamp, H., Stronks, K., Snijder, M. B., & Derkx, E. M. (2017). Measurement invariance testing of the PHQ-9 in a multi-ethnic population in europe: The HELIUS study. *BMC Psychiatry*, 17, 1–14.
- Gruebner, O., Rapp, M. A., Adli, M., Kluge, U., Galea, S., & Heinz, A. (2017). Cities and mental health. *Deutsches Ärzteblatt International*, 114(8), 121.
- Howlett, R. J. (2001). *Radial basis function networks 1: Recent developments in theory and applications*.
- Hyttinen, A., Eberhardt, F., & Hoyer, P. O. (2012). Learning linear cyclic causal models with latent variables. *The Journal of Machine Learning Research*, 13(1), 3387–3439.
- Kroenke, K., Spitzer, R. L., & Williams, J. B. (2001). The PHQ-9: Validity of a brief depression severity measure. *Journal of General Internal Medicine*, 16(9), 606–613.
- Leemput, I. A. van de, Wichers, M., Cramer, A. O., Borsboom, D., Tuerlinckx, F., Kuppens, P., Van Nes, E. H., Viechtbauer, W., Giltay, E. J., Aggen, S. H., et al. (2014). Critical slowing down as early warning for the onset and termination of depression. *Proceedings of the National Academy of Sciences*, 111(1), 87–92.
- Lindsay, B. G., Pilla, R. S., & Basak, P. (2000). Moment-based approximations of distributions using mixtures: Theory and applications. *Annals of the Institute of Statistical Mathematics*, 52, 215–230.
- Lorant, V., Deliège, D., Eaton, W., Robert, A., Philippot, P., & Ansseau, M. (2003). Socioeconomic inequalities in depression: A meta-analysis. *American Journal of Epidemiology*, 157(2), 98–112.
- Lund, C., Breen, A., Flisher, A. J., Kakuma, R., Corrigall, J., Joska, J. A., Swartz, L., & Patel, V. (2010). Poverty and common mental disorders in low and middle income countries: A systematic review. *Social Science & Medicine*, 71(3), 517–528.
- Lund, C., Brooke-Sumner, C., Baingana, F., Baron, E. C., Breuer, E., Chandra, P., Haushofer, J., Herrman, H., Jordans, M., Kieling, C., et al. (2018). Social determinants of mental disorders and the sustainable development goals: A systematic review of reviews. *The Lancet Psychiatry*, 5(4), 357–369.

- McDaid, D., Park, A.-L., & Wahlbeck, K. (2019). The economic case for the prevention of mental illness. *Annual Review of Public Health*, 40(1), 373–389.
- McKee, M., Reeves, A., Clair, A., & Stuckler, D. (2017). Living on the edge: Precariousness and why it matters for health. *Archives of Public Health*, 75, 1–10.
- Mooij, J. M., & Claassen, T. (2020). Constraint-based causal discovery using partial ancestral graphs in the presence of cycles. *Conference on Uncertainty in Artificial Intelligence*, 1159–1168.
- Neapolitan, R. E. et al. (2004). *Learning bayesian networks* (Vol. 38). Pearson Prentice Hall Upper Saddle River.
- Park, K., Li, X., Waldorp, L., Lees, M., & Vasconcelos, V. V. (2025). *The role of feedback loops in dynamical symptom networks*.
- Park, K., Waldorp, L. J., & Ryan, O. (2024). Discovering cyclic causal models in psychological research. *Advances. In/Psychology*, 2, e72425.
- Park, K., Waldorp, L., & Vasconcelos, V. V. (2025). *The individual-and population-level mechanistic implications of statistical networks of symptoms*.
- Pevalin, D. J., Reeves, A., Baker, E., & Bentley, R. (2017). The impact of persistent poor housing conditions on mental health: A longitudinal population-based study. *Preventive Medicine*, 105, 304–310.
- Rahimi, A., & Recht, B. (2007). Random features for large-scale kernel machines. *Advances in Neural Information Processing Systems*, 20.
- Rehm, J., & Shield, K. D. (2019). Global burden of disease and the impact of mental and addictive disorders. *Current Psychiatry Reports*, 21, 1–7.
- Ridley, M., Rao, G., Schilbach, F., & Patel, V. (2020). Poverty, depression, and anxiety: Causal evidence and mechanisms. *Science*, 370(6522), eaay0214.
- Rohbeck, M., Clarke, B., Mikulik, K., Pettet, A., Stegle, O., & Ueltzhöffer, K. (2024). Bicycle: Intervention-based causal discovery with cycles. In F. Locatello & V. Didelez (Eds.), *Proceedings of the third conference on causal learning and reasoning* (Vol. 236, pp. 209–242). PMLR.
- Rönnblad, T., Grönholm, E., Jonsson, J., Koranyi, I., Orellana, C., Kreshpaj, B., Chen, L., Stockfelt, L., & Bodin, T. (2019). Precarious employment and mental health. *Scandinavian Journal of Work, Environment & Health*, 45(5), 429–443.
- Rugulies, R., Aust, B., Greiner, B. A., Arensman, E., Kawakami, N., LaMontagne, A. D., & Madsen, I. E. (2023). Work-related causes of mental health conditions and interventions for their improvement in workplaces. *The Lancet*, 402(10410), 1368–1381.
- Runge, J., Nowack, P., Kretschmer, M., Flaxman, S., & Sejdinovic, D. (2019). Detecting and quantifying causal associations in large nonlinear time series datasets. *Science Advances*, 5(11), eaau4996.
- Savigny, D. de, & Adam, T. (Eds.). (2009). *Systems thinking for health systems strengthening*. Alliance for Health Policy; Systems Research, World Health Organization.
- Sethuraman, M. G., Lopez, R., Mohan, R., Fekri, F., Biancalani, T., & Hütter, J.-C. (2023). NODAGS-flow: Nonlinear cyclic causal structure learning. *International Conference on Artificial Intelligence and Statistics*, 6371–6387.
- Snijder, M. B., Galenkamp, H., Prins, M., Derkx, E. M., Peters, R. J., Zwinderman, A. H., & Stronks, K. (2017). Cohort profile: The healthy life in an urban setting (HELIUS) study in amsterdam, the netherlands. *BMJ Open*, 7(12), e017873.

- Spirites, P., Glymour, C., & Scheines, R. (2001). *Causation, prediction, and search*. MIT press.
- Spirites, P., Meek, C., & Richardson, T. (1995). Causal inference in the presence of latent variables and selection bias. *Proceedings of the Eleventh Conference on Uncertainty in Artificial Intelligence*, 499–506.
- Storn, R., & Price, K. (1997). Differential evolution—a simple and efficient heuristic for global optimization over continuous spaces. *Journal of Global Optimization*, 11, 341–359.
- Strobl, E. V. (2019). A constraint-based algorithm for causal discovery with cycles, latent variables and selection bias. *International Journal of Data Science and Analytics*, 8(1), 33–56. <https://doi.org/10.1007/s41060-018-0158-2>
- Strobl, E. V., Zhang, K., & Visweswaran, S. (2019). Approximate kernel-based conditional independence tests for fast non-parametric causal discovery. *Journal of Causal Inference*, 7(1), 20180017.
- Stronks, K., Snijder, M. B., Peters, R. J., Prins, M., Schene, A. H., & Zwinderman, A. H. (2013). Unravelling the impact of ethnicity on health in europe: The HELIUS study. *BMC Public Health*, 13, 1–10.
- Van Der Wal, J. M., Van Borkulo, C. D., Deserno, M. K., Breedvelt, J. J., Lees, M., Lokman, J. C., Borsboom, D., Denys, D., Holst, R. J. van, Smidt, M. P., et al. (2021). Advancing urban mental health research: From complexity science to actionable targets for intervention. *The Lancet Psychiatry*, 8(11), 991–1000.
- Wagenaar, A. C., & Burris, S. (2013). *Public health law research: Theory and methods*. John Wiley & Sons.
- Weich, S., & Lewis, G. (1998). Poverty, unemployment, and common mental disorders: Population based cohort study. *Bmj*, 317(7151), 115–119.
- Wichers, M., Groot, P. C., Psychosystems, E., Group, E., et al. (2016). Critical slowing down as a personalized early warning signal for depression. *Psychotherapy and Psychosomatics*, 85(2), 114–116.
- World Health Organization. (2022). *Mental disorders*. World Health Organization. <https://www.who.int/news-room/fact-sheets/detail/mental-disorders>
- Zawadzki, M. J., Graham, J. E., & Gerin, W. (2013). Rumination and anxiety mediate the effect of loneliness on depressed mood and sleep quality in college students. *Health Psychology*, 32(2), 212.
- Zhang, K., Peters, J., Janzing, D., & Schölkopf, B. (2012). Kernel-based conditional independence test and application in causal discovery. *arXiv Preprint arXiv:1202.3775*.

6 Appendix

6.1 HELIUS study

The HELIUS (HEalthy LIfe in an Urban Setting) study is a large-scale, multiethnic cohort study conducted in Amsterdam. Participants were randomly selected from the municipality register and stratified by ethnic origin to ensure balanced representation across six major groups. Invitation letters were sent by mail, followed by a reminder after two weeks. Non-respondents were contacted via home visits where applicable.

Of those invited, approximately 55% responded (Dutch: 55%, Surinamese: 62%, Ghanaian: 57%, Turkish: 46%, Moroccan: 48%). Among those contacted, 50% agreed to participate (Dutch: 60%, Surinamese: 51%, Ghanaian: 61%, Turkish: 41%, Moroccan: 43%), resulting in an overall participation rate of 28%.

Participants completed either a digital or paper version of the questionnaire, with assistance offered when needed, and received a confirmation letter for a physical examination appointment.

At baseline (2011–2015), 24,780 individuals were enrolled. Of these, 23,936 participants completed the questionnaire that included items relevant to precariousness. After excluding individuals with missing data on key variables, the final analytical sample consisted of 21,628 participants.

The HELIUS study received approval from the Medical Ethics Committee of the Academic Medical Center (AMC), and written informed consent was obtained from all participants prior to enrollment.

6.2 Causal Discovery Primer

As shown in Table 1, the resulting graphs from FCI and CCI differ slightly (*PAG*: partial ancestral graph; *MAAG*: maximal almost ancestral graph) due to their reliance on different underlying assumptions. Despite these differences, both graphs belong to the class of *ancestral graphs*, which are designed to encode causal relationships between variables, where the presence of an edge indicates causal *ancestry*. In these graphs, directed edges, $A^* \rightarrow B$, indicate that B is not an ancestor of A in every graph within the Markov equivalence class, $\text{Equiv}(G)$. The Markov equivalence class represents a set of graphs that encode the same conditional independence relationships, ensuring that the same *d-separation* conditions hold across all graphs in the class (Spirtes et al., 2001). Conversely, an edge marked as $A^* \leftarrow B$ indicates that B is an ancestor of A across all graphs in $\text{Equiv}(G)$. Circle endpoints, $A^* \circ B$, represent ambiguity in the ancestral relationship, meaning B 's ancestral status relative to A varies across graphs in $\text{Equiv}(G)$.² Finally, when an edge is represented as $A \leftrightarrow B$, it implies that neither A nor B is an ancestor of the other, suggesting the presence of a latent confounder influencing both variables.

The algorithms also differ in how they detect cycles and represent cyclic relationships in their resulting graphs. In CCI's MAAG, $A — B$ indicates that A is an ancestor of B , and simultaneously B is an ancestor of A , referring to a cyclic relationship between $A \leftarrow B$. FCI, on the other hand, identifies potential cycles more subtly. In its PAG, fully-connected nodes with circle endpoints ($\circ\circ$) may suggest the presence of cyclic structures. FCI, therefore, provides a sufficient condition to distinguish variables that are not part of a cycle, offering a more nuanced approach to handling cyclic relationships (Mooij & Claassen, 2020).

Table 1 highlights further differences in the assumptions underlying these algorithms. CCI operates under the assumption of a linear system, whereas FCI,

²* serves as a *meta-symbol*, representing one of the three possible edge-endpoints. For instance, $A^* \leftarrow B$ can indicate any of the following edges: $A — B$, $A \rightarrow B$, or $A \circ B$ (Park et al., 2024).

Table 1: Assumptions of causal discovery algorithms

Algorithm	Acylicity	Causal sufficiency	Absence of selection bias	Linearity	Output
PC	✓	✓	✓	✓	CPDAG
FCI	— ^a	✓	— ^a	— ^a	PAG
CCI	✗	✗	✗	✓	(partially oriented) MAAG

Note. ^aThe FCI algorithm, introduced by Spirtes (1995), is a constraint-based causal discovery method for DAGs that accounts for latent confounding and selection bias. Mooij & Claassen (2020) later showed its applicability to cyclic causal discovery with latent confounding under general faithfulness and Markov conditions, assuming non-linear causal relationships.

particularly when used to infer cyclic relationships, assumes a non-linear system without selection bias and adheres to more general faithfulness and Markov conditions (i.e., σ -separation and σ -faithfulness setting) (Forré & Mooij, 2018). When the respective assumptions of each algorithm are met, their inferred cyclic relationships align with those illustrated in Figure 9.

While CCI’s MAAG provides an explicit representation of cyclic relationships, it has certain theoretical limitations, as the MAAG may not always fully preserve d-separation relations from the original graph, \mathcal{G} (Strobl, 2019). Given these considerations, we examine and compare results from both algorithms, placing more weight on the FCI results, which are presented in the main results section, while discussing CCI results where relevant, with detailed findings provided in Section 6.4. A full discussion of causal discovery concepts and algorithmic details is beyond the scope of this paper; however, readers seeking a more in-depth understanding can refer to Park et al. (2024) for a comprehensive exploration of these methods and their applications.

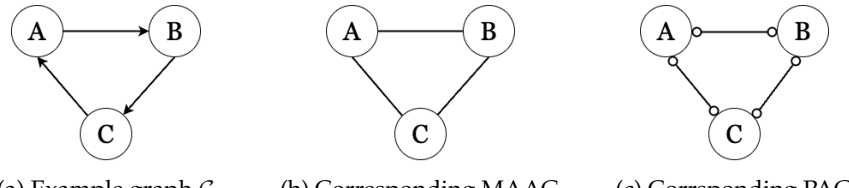


Figure 9: Example graph \mathcal{G} featuring a cycle and the corresponding MAAG from CCI and PAG from FCI.

The graph produced by the PC algorithm is a CPDAG (completed partially directed acyclic graph), where directed edges ($A \rightarrow B$) indicate that A is a direct cause (parent) of B . Unlike FCI and CCI, the CPDAG does not include circle symbols. Instead, when the PC algorithm cannot determine the direction of causality, it represents this uncertainty with bidirectional arrows. While the PC algorithm serves as a useful reference, its strict assumptions —acyclicity and the absence of latent confounders—limit its applicability in more complex scenarios. For this

reason, our primary focus remains on the results obtained from FCI and CCI, with all PC algorithm results provided in Section 6.5 for completeness.

6.3 Precariousness Domains Based on Elsenburg et al. (2025)

1. EMPLOYMENT PRECARIOUSNESS

- H1_Arbeidsparticipatie: Working status
- H1_WerkSIt: Which work situation most applies to you?
- H1_RecentErv8: Experiences past 12 months: h. You were sacked from your job or became unemployed (*reverse*)

2. FINANCIAL PRECARIOUSNESS

- H1_InkHhMoeite: During the past year, did you have problems managing your household income?
- H1_RecentErv9: Experiences past 12 months: i. You had a major financial crisis (*reverse*)

3. HOUSING PRECARIOUSNESS

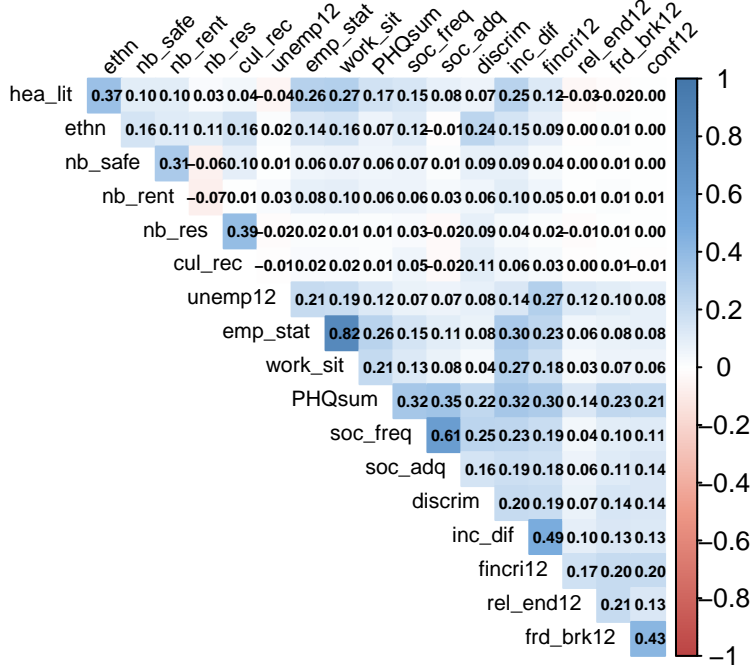
- veilig_2012: Score safety (veiligheid) in 2012 (*reverse*)
- vrz_2012: Score level of resources (niveau voorzieningen) in 2012 (*reverse*)
- P_HUURWON: Percentage Huurwoningen

4. CULTURAL PRECARIOUSNESS

- H1_Discr_sumscore: Perceived discrimination: sum score of 9 items (range 9-45)
- H1_SBSQ_meanscore: Health literacy: SBSQ meanscore (range 1-5) (*reverse*)
- A_BED_RU: Aantal bedrijfsvestigingen; cultuur, recreatie, overige diensten (*reverse*)

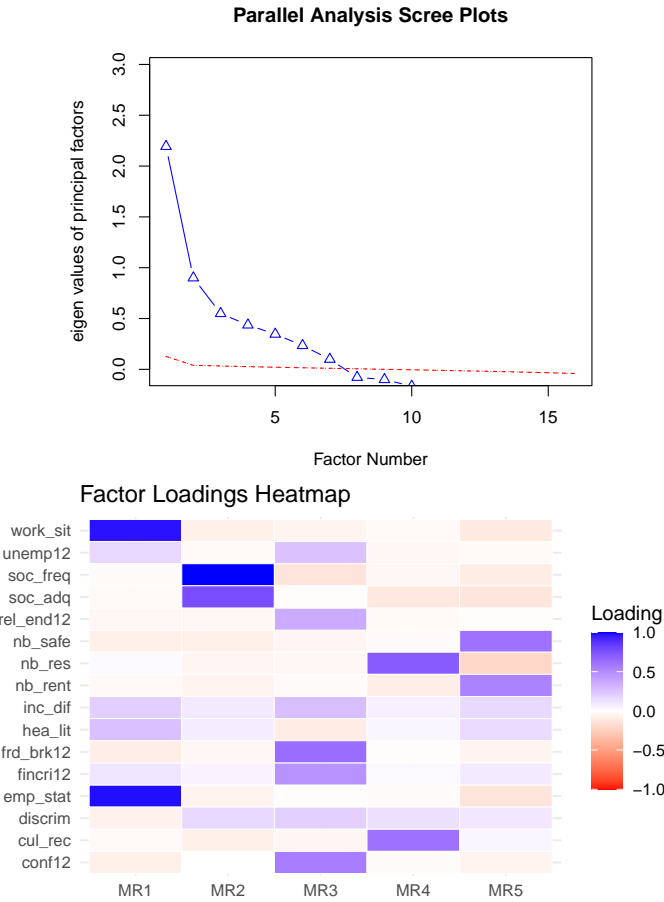
5. SOCIAL PRECARIOUSNESS

- H1_RecentErv5: Experiences past 12 months: e. Your steady relationship ended (*reverse*)
- H1_RecentErv6: Experiences past 12 months: f. A long-term friendship with a good friend or family member was broken off (*reverse*)
- H1_RecentErv7: Experiences past 12 months: g. You had a serious problem with a good friend or family member, or neighbour (*reverse*)
- H1_SSQT: SSQT (frequency of social contact): sum score of 5 items (range 5-20) (*reverse*)
- H1_SSQSa: SSQS (adequacy of social contact): sum score of 5 items, category 3 and 4 not combined (range 5-20) (*reverse*)



- High Correlations:** `emp_stat` (employment status) and `work_sit` (work situation) have a strong positive correlation of 0.82. This suggests that individuals with higher employment status tend to have more secure or favorable work situations. `soc_freq` (social contact frequency) shows a strong positive correlation with `soc_adq` (social adequacy) at 0.61. This indicates that individuals with more frequent social contact also tend to have higher perceived adequacy of social interactions.
- Moderate Correlations:** `nb_safe` (neighborhood safety) and `nb_res` (resources) have a moderate positive correlation of 0.39, suggesting that areas with higher safety also have better resources. `hea_lit` (health literacy) has moderate correlations with `emp_stat` (0.26) and `work_sit` (0.25), which could mean that higher health literacy is associated with better employment situations. `frd_brk12` (friendship breakups) and `conf12` (conflicts) have a notable correlation of 0.43, indicating a relationship between having conflicts and friendship losses.
- Low to Moderate Correlations in Financial Precariousness:** `inc_dif` (income difficulties) has a moderate correlation with `fincri12` (financial crisis) at 0.49. This aligns with the expected relationship, where individuals who experience general income difficulties are more likely to report financial crises.
- Low Correlations (0.1 - 0.2):** Many variables, such as `discrim` (discrimination), `unemp12` (unemployment experience), and `rel_end12` (relationship end), have low correlations with other variables, suggesting relatively independent relationships in the context of this dataset.

6.3.1 Exploratory Factor Analysis (EFA)



6.3.1.1 Factor Loadings (Pattern Matrix)

- **MR1:** High loadings on `emp_stat` and `work_sit` suggest this factor captures *employment precariousness*.
- **MR2:** Strong loadings on `soc_freq` and `soc_adq` indicate *social precariousness*.
- **MR3:** Key items like `frd_brk12`, `conf12`, and `fincri12`, suggest recent *stressful events*.
- **MR4:** High loadings on `nb_res` and `cul_rec` may reflect *community resources precariousness*.
- **MR5:** Variables `nb_safe` and `nb_rent` with high loadings indicate *housing precariousness*.

6.3.1.2 Variance Explained

The factors cumulatively explain 38% of the variance, with MR1 being the most influential factor. Each factor contributes a smaller proportion to the total variance

(MR1 at 12%, MR2 at 9%, etc.).

6.3.1.3 Factor Intercorrelations

Factors are moderately correlated, especially between *MR1 and MR5*, and *MR2 and MR3*. This indicates that while distinct, these factors are related—reasonable in a complex socio-economic context.

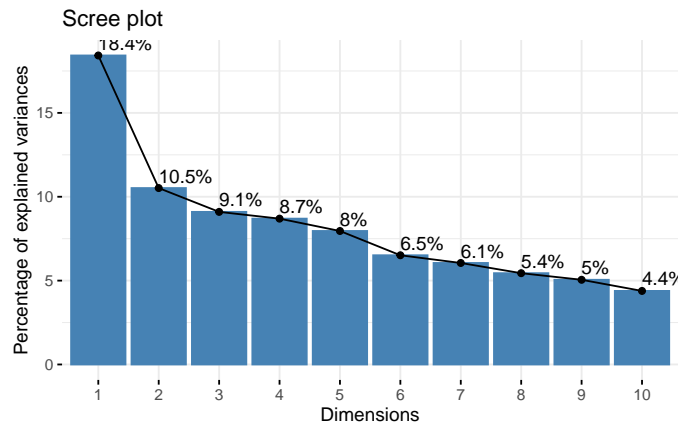
6.3.1.4 Model Fit Statistics

RMSEA (0.071) suggest an acceptable fit. Tucker Lewis Index (0.802) suggests moderate reliability for the model.

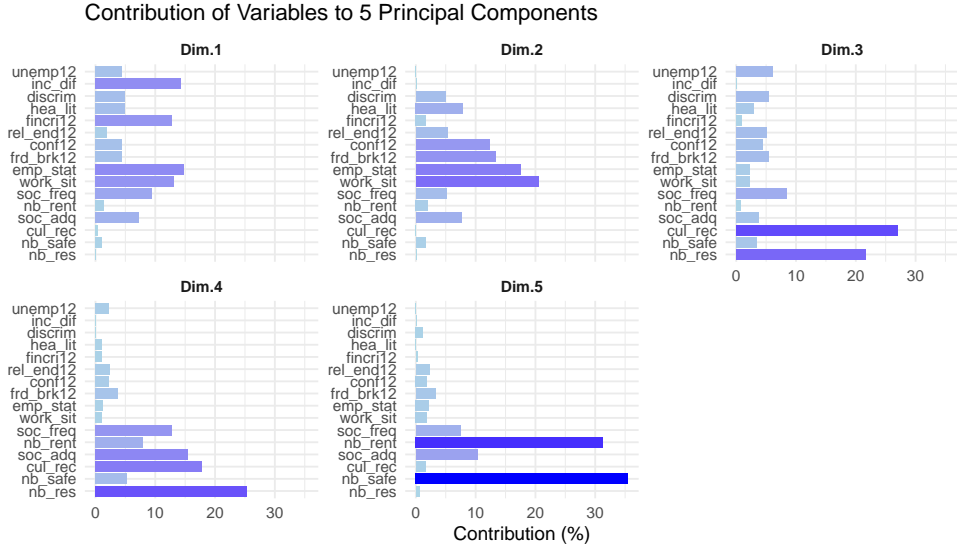
6.3.1.5 Summary

The 5-factor model appears interpretable and captures distinct dimensions of precariousness: *employment, social, stressors, community resources, and housing precariousness*. Although the overall fit and explained variance could be stronger, these factors offer insights into the underlying structure of the data, highlighting key areas of precariousness.

6.3.2 PCA



- Component Retention: The scree plot shows a clear “elbow” after the first component. This steep drop suggests that most variance is explained by the first component. After Dimension 5, the percentage of explained variance decreases slightly more gradually, indicating diminishing returns for adding more components. If we need to choose multiple components, retaining the first 5 components seems reasonable, as they capture most of the variance (cumulatively explaining about 54.7% of the total variance).



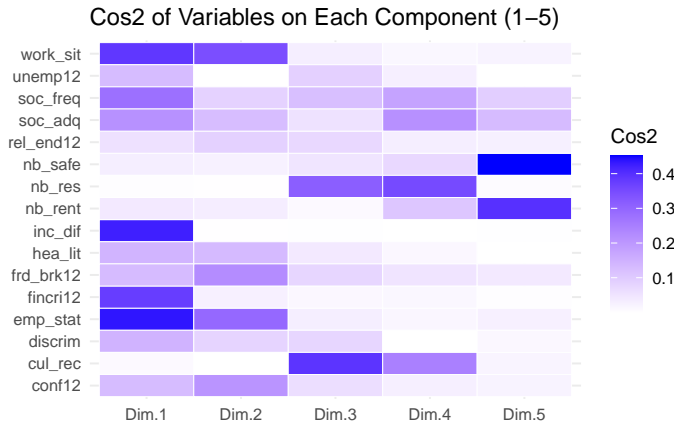
6.3.2.1 Explained variance (contributions) of variables

It shows the importance of variables within each component.

- **Dim1:** High contributions are observed from `emp_stat`, `work_sit`, `inc_dif`, and `fincri12`, suggesting that this dimension captures aspects of *employment and financial security*.
- **Dim2:** While `emp_stat` and `work_sit` overlap with Dim1, the strong contributions from `frd_brk12` and `rel_end12` indicate that this dimension captures a focus on *recent relationship stressors*.
- **Dim3:** `cul_rec`, `nb_res` have the highest contributions, indicating this dimension likely represents *community and cultural factors*.
- **Dim4:** `soc_freq` and `soc_adq` stand out in this dimension, suggesting an emphasis on *social precariousness*.
- **Dim5:** `nb_safe` and `nb_rent` are the top contributors, pointing to *housing security* as key themes in this component.

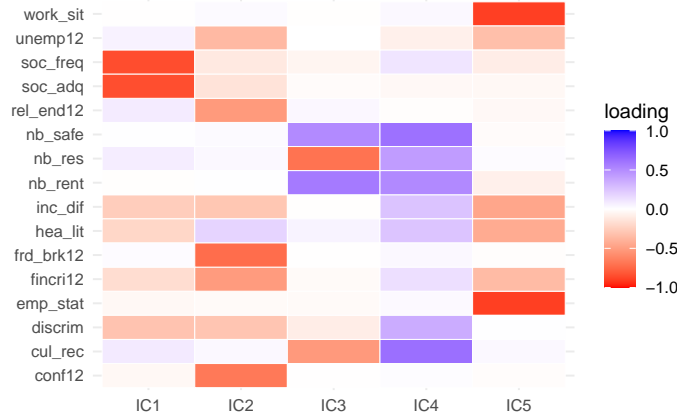
6.3.2.2 Cos² Values

Cos² (squared cosine) values, or the quality of representation, show how well each variable is represented by each dimension. where higher cos² values (closer to 1) indicate better representation of a variable by a component.



- **Dim.1:** Variables `emp_stat`, `work_sit`, `inc_dif`, and `fincri12` show high \cos^2 values, meaning that PC1 primarily captures variations in employment and financial difficulties. This component could represent *employment & finance* precariousness.
- **Dim.2:** Variables `work_sit`, `emp_stat`, `frd_brk12`, and `conf12` are well-represented in this component, suggesting PC2 captures aspects of *recent relationship stressors*.
- **Dim.3:** Variables `nb_res` and `cul_rec` load strongly on PC3. This may represent community or cultural resources, indicating that this component is associated with *neighborhood resources*.
- **Dim.4:** This component has high \cos^2 values for `nb_res`, `cul_rec`, `soc_freq`, and `soc_adq`. While `nb_res` and `cul_rec` are also prominent in PC3, PC4 uniquely captures nuanced differentiation in *social* precariousness.
- **Dim.5:** `nb_safe` and `nb_rent` are well-represented by PC5. This component might capture *housing* precariousness.

6.3.3 ICA



6.3.3.1 Dominant Variables per Component:

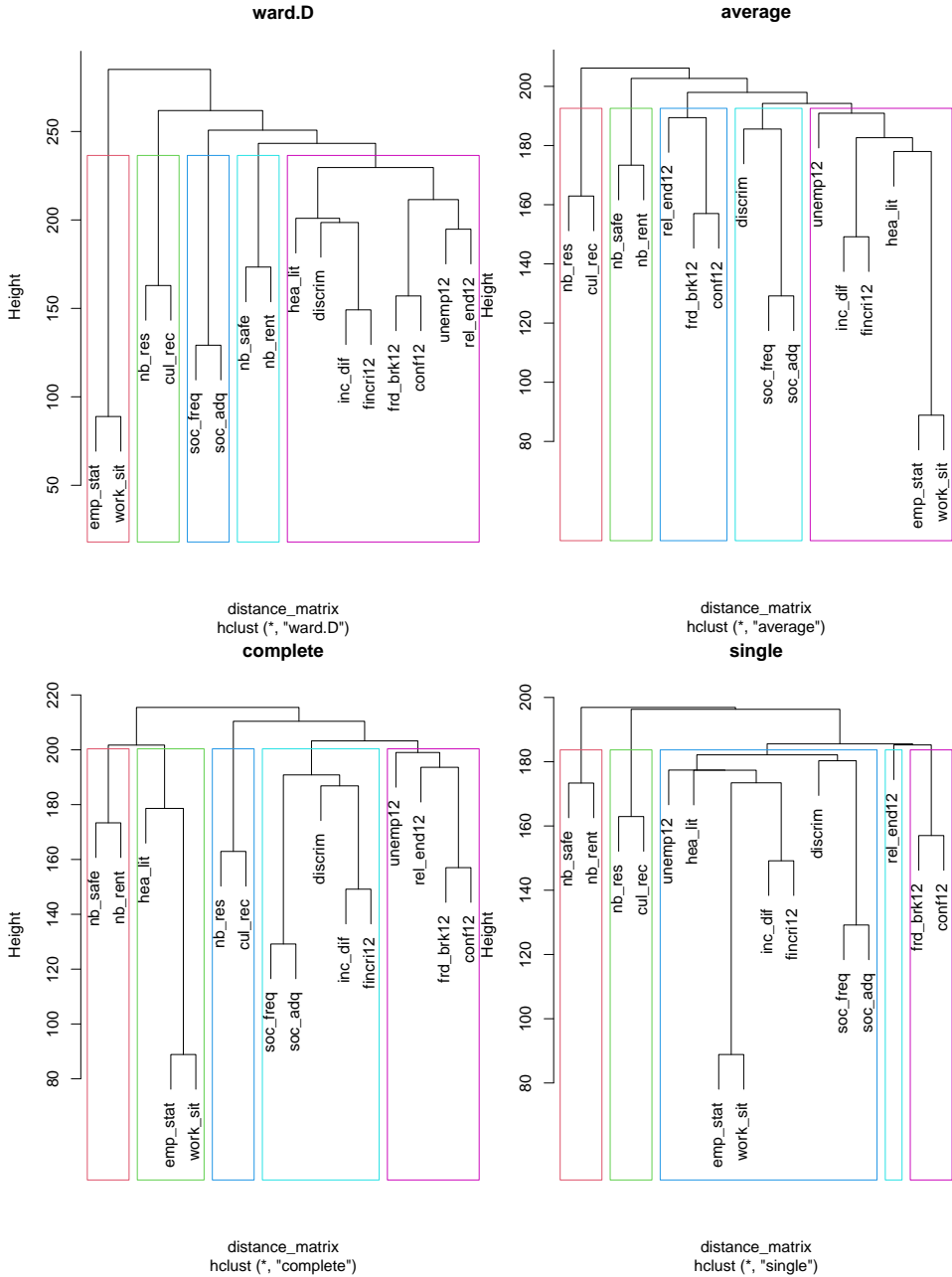
For each Independent Component (IC), we can identify variables with *high absolute* values in each column. These values indicate that the IC captures a strong, independent signal associated with these variables.

- **IC1:** *soc_freq* and *soc_adq* have strong negative loadings on this component, indicating that this component might represent *social precariousness*.
- **IC2:** *frd_brk12*, *conf12*, *rel_end12*, *fincri12* and *unemp12* have the most substantial loadings on this component, all with negative signs. This might point to a *recent relational or social stressor* component.
- **IC3:** *nb_res* and *cul_rec* show notable negative loadings, pointing to a focus on *community resource precariousness*.
- **IC4:** High loadings for *nb_safe*, *nb_rent*, *nb_res*, *cul_rec*, and *discrim* suggest a theme of *housing and community-based precariousness*, reflecting both safety and social challenges within the neighborhood context.
- **IC5:** *emp_stat* and *work_sit* both have strong negative loadings on this component, suggesting it captures *employment precariousness*.

6.3.4 Hierarchical clustering

6.3.4.1 Using Euclidean distance

- Ward.D's method: Minimizes the variance within clusters, producing more compact and spherical clusters.
- Single linkage: Groups clusters based on the minimum distance between points.
- Complete linkage: Groups clusters based on the maximum distance between points.
- Average linkage: Uses the average distance between all pairs of points in the two clusters.



6.3.4.1.1 Consistent Groupings (Across All or Most Methods)

- `emp_stat` and `work_sit`: This pair consistently clusters together across all linkage methods, suggesting that they are closely related variables, likely capturing a similar aspect of the data (possibly employment status or employment-related information).
- `nb_safe`, `nb_res`, and `nb_rent`: These variables are often grouped closely in several methods (especially Ward.D, average, and complete linkage). This suggests a similarity or common theme among them, potentially related to neighborhood or housing precariousness.
- `soc_freq` and `soc_adq`: These two variables frequently cluster together, indicating they likely measure aspects of social frequency and adequacy in similar ways. They appear together in Ward.D, average, and complete linkage.
- `frd_brk12` and `conf12`: These variables are often clustered closely (though they sometimes join with other variables like `rel_end12`), suggesting they may capture aspects of relationship or social conflict. This pair appears in close proximity, especially in average and Ward.D.

6.3.4.1.2 Inconsistent Groupings (Variability Across Methods)

- `hea_lit`: This variable shows inconsistent clustering across methods. In Ward.D, it joins with `fincril12`, while in other methods, it's often more isolated or grouped with variables that do not appear similar. This may suggest that `hea_lit` does not strongly correlate with other variables, or it has multidimensional aspects affecting its grouping across methods.
- `discrim`: This variable also shows variable groupings. In Ward.D, it is grouped with `hea_lit`, while in other methods (e.g., complete and single linkage), it clusters differently, sometimes on its own. This variability may indicate that `discrim` has weaker associations with the main clusters in the data or overlaps partially with multiple clusters.
- Social and Financial Variables (`inc_dif`, `fincril12`, `unemp12`): These variables appear together in some methods (e.g., Ward.D clusters `fincril12` and `inc_dif`), but in others, they are spread out. This inconsistency suggests that social and financial variables may not have strong or consistent ties across different methods, perhaps due to capturing different aspects of precariousness.

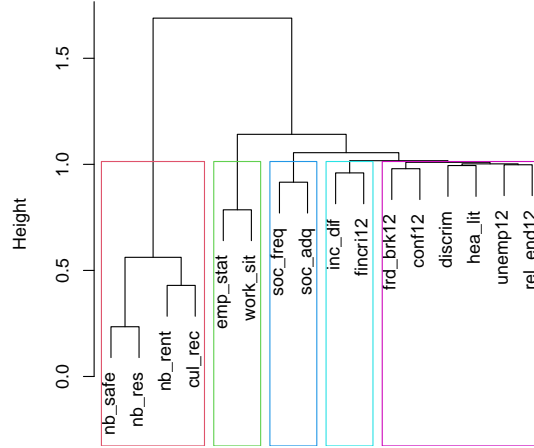
6.3.4.1.3 Summary

The consistent clusters are likely capturing distinct thematic dimensions of the data (e.g., employment, housing, social contact), while the inconsistent variables may reflect multifaceted or weakly correlated attributes that do not fit neatly into one cluster.

6.3.4.2 Using Mutual Information

Using mutual information (MI) as a basis for hierarchical clustering differs from using traditional distance measures (like Euclidean distance) in a few key ways.

Hierarchical Clustering (Mutual Information Distance)



6.3.4.2.1 Comparison to Euclidean Distance Clustering

- **Housing and Community Cluster:** The variables `nb_safe`, `nb_res`, `nb_rent`, and `cul_rec` cluster together, indicating a strong association among housing-related and community-based factors. This suggests a shared theme of housing or community precariousness. This grouping is also observed in the Euclidean-based clustering, but it appears more tightly connected here, potentially due to the non-linear relationships highlighted by mutual information.
- **Employment and Social Support Cluster:** `emp_stat` and `work_sit` form a cluster, linking employment status and work situation together as they did in Euclidean-based clustering. These remain closely associated regardless of the distance metric used. `soc_freq` and `soc_adq`, related to social contact frequency and adequacy, cluster nearby, indicating they have a stronger non-linear relationship with employment variables. This is a subtle difference as Euclidean distance might not capture this association as effectively.
- **Financial Stressor Cluster:** `inc_dif` and `fincri12`, representing income difficulties and recent financial crises, consistently cluster together in both approaches, showing a strong association, likely linear. However, mutual information-based clustering links these financial stressors with social support variables, suggesting that financial challenges may have complex dependencies with social support in this dataset.
- **Relational Stressor Cluster:** `frd_brk12`, `conf12`, `discrim`, `hea_lit`, `unemp12`, and `rel_end12` form a *looser* cluster focused on social and relational stressors (e.g., friendship breakup, conflicts, and discrimination).

Compared to Euclidean clustering, `discrim` and `hea_lit` (health literacy) appear closer to relational stressors here, indicating that non-linear relationships might play a larger role in linking these variables.

6.3.4.2.2 Summary

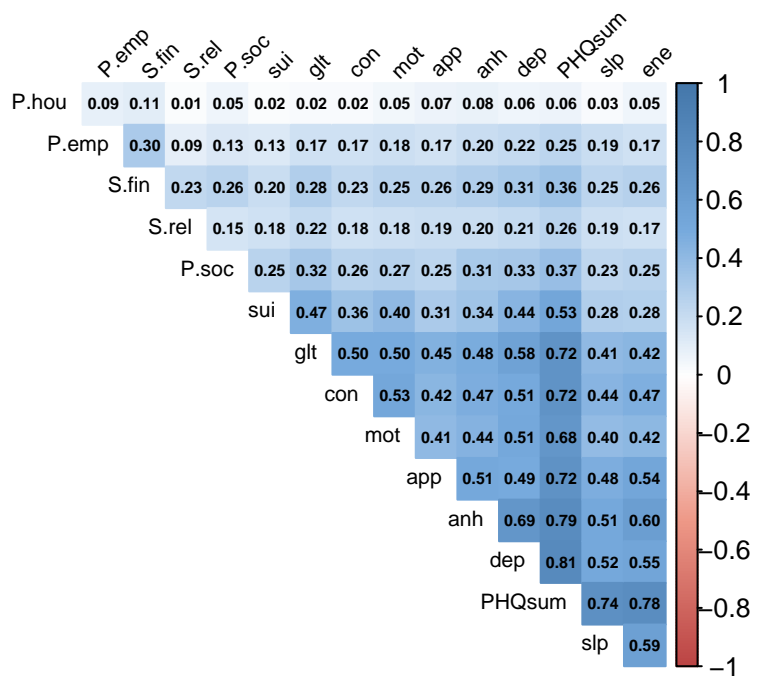
In conclusion, mutual information-based clustering provides an alternative perspective that can reveal more intricate associations between variables, especially for those with non-linear relationships. Compared to Euclidean clustering, it shows a similar high-level structure but emphasizes nuanced connections between variables, particularly around social support, employment, and financial stress.

6.3.5 Conclusions on Precariousness factors

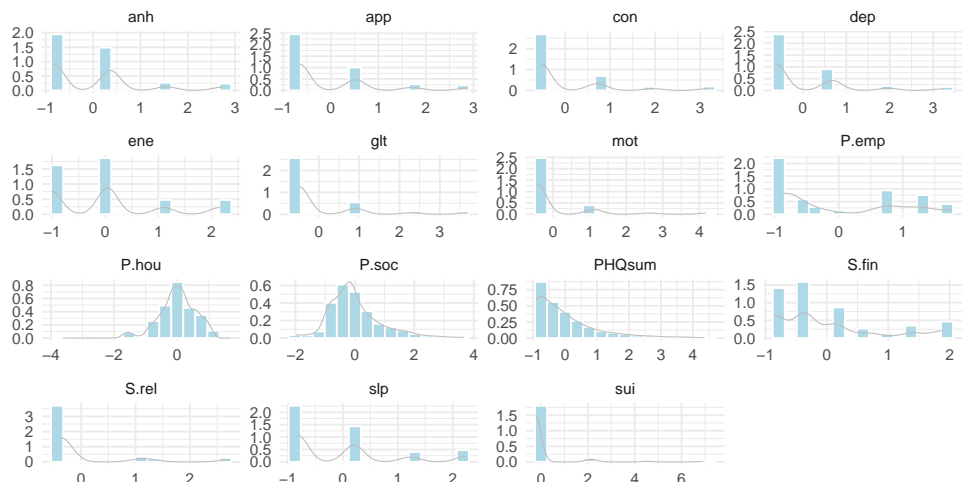
Based on the consistent findings across multiple analyses, we decided to exclude the variables `discrim`, `hea_lit`, `umemp12`, and `rel_end12`, as they do not clearly belong to any specific precariousness factor nor exhibit strong associations with depression (see the correlation table above). Therefore, we propose retaining the following key precariousness factors:

- Employment Precariousness: `emp_stat`, `work_sit`
- Social Precariousness: `soc_freq`, `soc_adq`
- Housing Precariousness: `nb_safe`, `nb_res`, `nb_rent`, `cul_rec`
- Recent Relational Stressors: `frd_brk12`, `conf12`
- Recent Financial Stressors: `fincr12`, `inc_diff`

We construct each precariousness factor by calculating the mean value of the combined variables. Below, we present the updated correlation table for the newly composed factors, along with the corresponding distributions of all variables to be used in the causal discovery analysis.



Distribution of All Variables with Density Overlay



6.4 Results from CCI algorithm

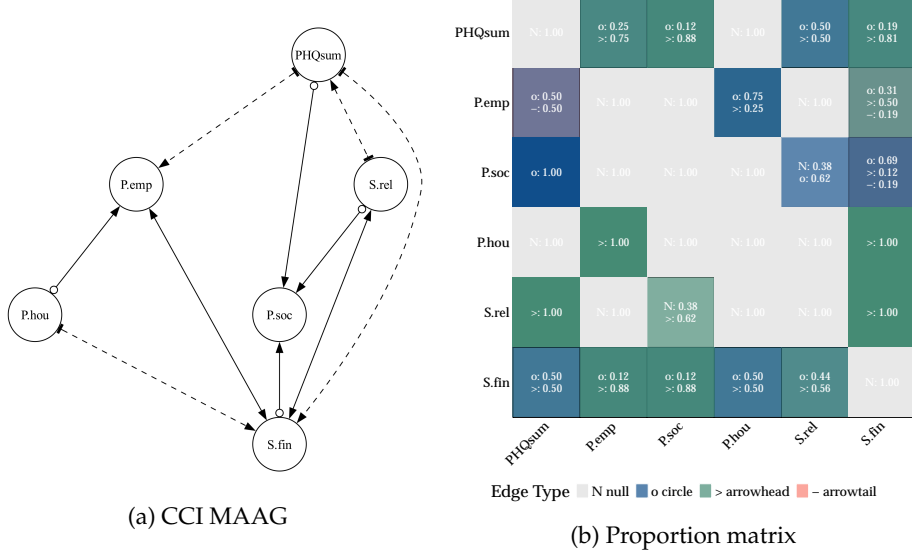
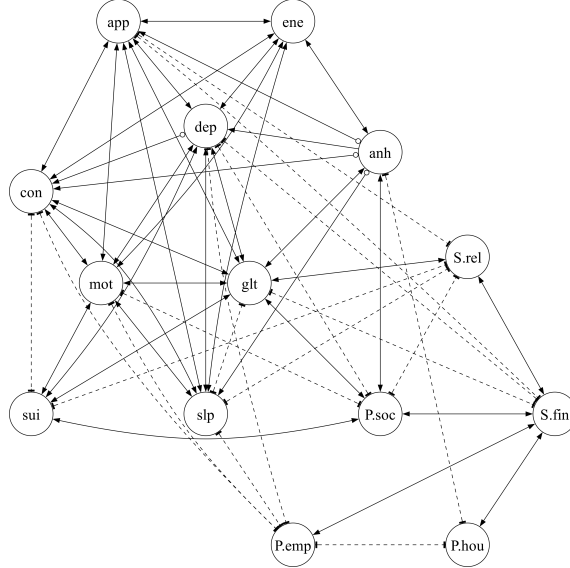


Figure 10: Resulting graph of precariousness factors and depression sum score using CCI and proportion of edge endpoint types.



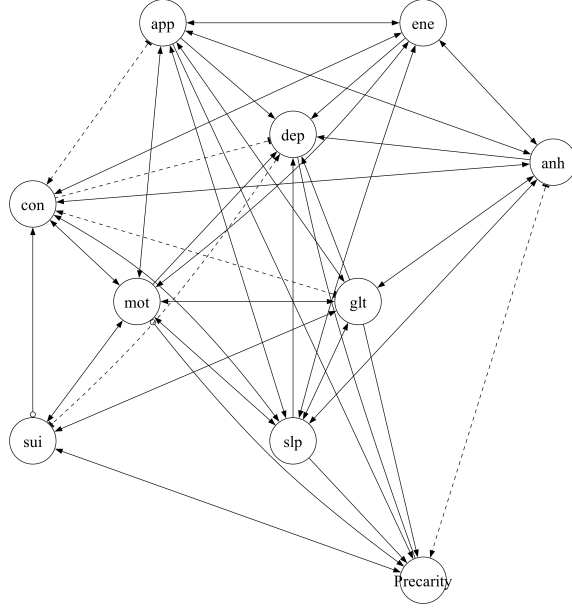
(a) CCI MAAG

	anh	dep	slp	ene	app	glt	con	mot	sui	P.emp	Psoc	Phou	S.rel	S.fin
anh	N: 1.00	> 1.00	> 1.00	> 1.00	> 1.00	N: 0.25 > 0.75	> 1.00	> 1.00	N: 1.00	N: 1.00	> 1.00	N: 0.50 > 0.50	N: 0.50 > 0.50	N: 1.00 > 0.50
dep	> 1.00	N: 1.00	> 1.00	N: 0.25 > 0.75	> 1.00	> 1.00	> 1.00	> 1.00	N: 1.00	N: 1.00	N: 1.00	N: 1.00 > 0.50	N: 1.00 > 0.50	N: 1.00 > 0.50
slp	> 1.00	> 1.00	N: 1.00	> 1.00	N: 0.50 > 0.50	> 1.00	> 1.00	> 1.00	N: 1.00	N: 1.00	N: 1.00	N: 1.00 > 0.50	N: 1.00 > 0.50	N: 0.75 > 0.25
ene	> 1.00	> 1.00	> 1.00	N: 1.00	> 1.00	> 1.00	> 1.00	> 1.00	N: 1.00	N: 1.00	N: 1.00	N: 1.00 > 0.50	N: 1.00 > 0.50	N: 0.50 > 0.50
app	> 1.00	N: 0.25 > 0.75	> 1.00	> 1.00	N: 1.00	> 1.00	> 1.00	> 1.00	N: 1.00	N: 1.00	N: 1.00	N: 0.50 > 0.50	N: 0.50 > 0.50	N: 0.50 > 0.50
glt	N: 0.25 > 0.75	> 1.00	N: 0.50 > 0.50	N: 1.00	> 1.00	N: 1.00	> 1.00	> 1.00	N: 1.00	N: 1.00	N: 1.00	N: 0.50 > 0.50	N: 0.50 > 0.50	N: 0.50 > 0.50
con	> 1.00	> 1.00	> 1.00	> 1.00	> 1.00	N: 1.00	> 1.00	> 1.00	N: 1.00	N: 1.00	N: 1.00	N: 0.50 > 0.50	N: 1.00 > 0.50	N: 1.00 > 0.50
mot	N: 1.00	> 1.00	> 1.00	> 1.00	> 1.00	> 1.00	> 1.00	> 1.00	N: 1.00	N: 1.00	N: 1.00	N: 1.00 > 0.50	N: 1.00 > 0.50	N: 1.00 > 0.50
sui	N: 1.00	> 1.00	N: 1.00	N: 1.00	N: 1.00	> 1.00	N: 0.50 > 0.50	> 1.00	N: 1.00	N: 1.00	N: 1.00	N: 0.25 > 0.75	N: 1.00	N: 1.00
P.emp	N: 1.00	N: 0.50 > 0.50	N: 0.50 > 0.50	N: 1.00	N: 1.00	N: 1.00	N: 0.50 > 0.50	N: 0.50 > 0.50	N: 1.00	N: 1.00	N: 1.00	N: 0.50 > 0.50	N: 1.00	> 1.00
Psoc	> 1.00	N: 0.50 > 0.50	N: 1.00	N: 1.00	N: 1.00	> 1.00	N: 0.50 > 0.50	N: 0.50 > 0.50	N: 0.25 > 0.75	N: 0.88 > 0.12	N: 1.00	N: 1.00	N: 0.50 > 0.50	> 1.00
Phou	N: 0.50 > 0.50	N: 1.00	N: 1.00	N: 1.00	N: 1.00	N: 0.88 > 0.12	N: 1.00	N: 1.00	N: 1.00	N: 0.50 > 0.50	N: 1.00	N: 1.00	N: 1.00	N: 0.38 > 0.62
S.rel	N: 1.00	N: 1.00	N: 0.50 > 0.50	N: 0.75 > 0.25	N: 0.62 > 0.38	N: 0.50 > 0.50	N: 0.25 > 0.75	N: 1.00						
S.fin	N: 0.50 > 0.50	N: 0.50 > 0.50	N: 0.75 > 0.25	N: 0.62 > 0.38	N: 0.50 > 0.50	N: 0.25 > 0.75	N: 1.00							

Edge Type ■ nul ■ circle ■ > arrowhead ■ – arrowtail

(b) Proportion matrix

Figure 11: Resulting graph of precariousness factors and individual depression symptoms using CCI and proportion of edge endpoint types.



(a) CCI MAAG

	anh	> 1.00	> 1.00	> 1.00	> 1.00	N: 0.12 > 0.88	> 1.00	> 1.00	N: 1.00	N: 1.00	> 1.00	
dep	$\alpha: 0.12$ $-: 0.88$	N: 1.00	< 1.00	$\alpha: 0.25$ > 0.12 $-: 0.62$	< 1.00	< 1.00	< 1.00	< 1.00	< 1.00	< 1.00	$\alpha: 0.50$ > 0.50	$\alpha: 0.38$ $-: 0.62$
sui	> 1.00	> 1.00	N: 1.00	> 1.00	> 1.00	N: 0.25 > 0.75	> 1.00	> 1.00	N: 1.00	N: 1.00	> 1.00	
ene	> 1.00	> 1.00	> 1.00	N: 1.00	> 1.00	N: 1.00	> 1.00	> 1.00	N: 1.00	N: 1.00	> 1.00	
app	> 1.00	> 1.00	> 1.00	> 1.00	N: 1.00	> 1.00	> 1.00	> 1.00	N: 1.00	N: 1.00	> 1.00	
glt	N: 0.12 > 0.88	> 1.00	N: 0.25 > 0.75	N: 1.00	> 1.00	N: 1.00	> 1.00	> 1.00	> 1.00	> 1.00	> 1.00	> 1.00
con	$\alpha: 0.12$ > 0.50 $-: 0.38$	$\alpha: 0.50$ > 0.50	$\alpha: 0.25$ > 0.50 $-: 0.25$	$\alpha: 0.25$ > 0.75	$\alpha: 0.50$ > 0.50	$\alpha: 0.50$ > 0.50	N: 1.00	N: 1.00	$\alpha: 0.25$ > 0.50 $-: 0.25$	$\alpha: 0.50$ > 0.62 $-: 0.38$	$\alpha: 0.50$ > 0.12 $-: 0.12$	
mot	N: 1.00	> 1.00	> 1.00	> 1.00	> 1.00	> 1.00	> 1.00	> 1.00	N: 1.00	> 1.00	> 1.00	
sui	N: 1.00	> 1.00	N: 1.00	N: 1.00	N: 1.00	> 1.00	N: 0.25 > 0.75	> 1.00	N: 1.00	N: 1.00	> 1.00	
precarity	$\alpha: 0.50$ $-: 0.50$	$\alpha: 0.25$ > 0.12 $-: 0.62$	$\alpha: 0.12$ > 0.50 $-: 0.50$	N: 1.00	$\alpha: 0.25$ > 0.22 $-: 0.62$	$\alpha: 0.25$ > 0.12 $-: 0.62$	$\alpha: 0.50$ > 0.12 $-: 0.38$	$\alpha: 0.75$ > 0.25	$\alpha: 0.75$ > 0.62	$\alpha: 0.38$ > 0.62	N: 1.00	

Edge Type ■ N null ■ o circle ■ > arrowhead ■ - arrowtail

(b) Proportion matrix

Figure 12: Resulting graph of precariousness sum score and individual depression symptoms using CCI and proportion of edge endpoint types.

6.5 Results from PC algorithm

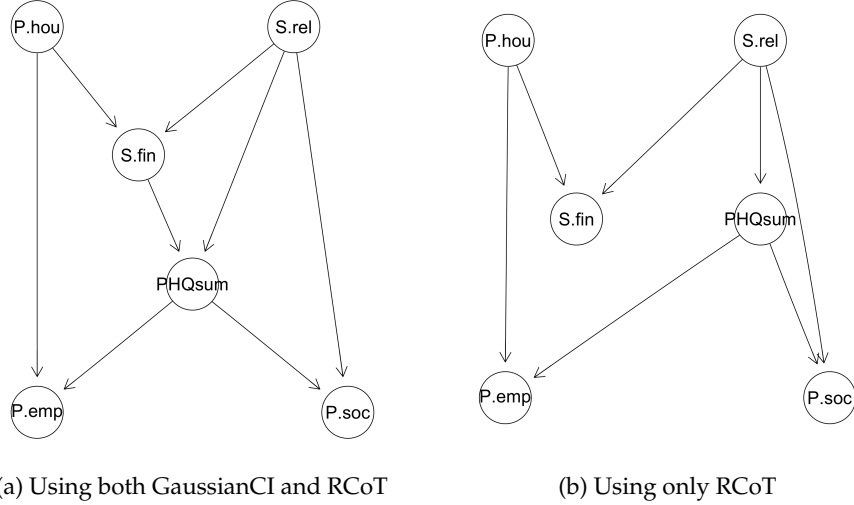


Figure 13: Resulting graphs of precariousness factors and depression sum score using PC.

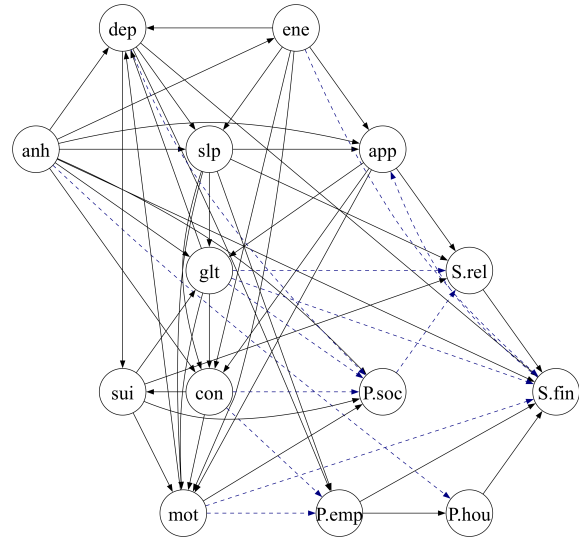


Figure 14: Resulting graphs of precariousness factors and individual depression symptoms using PC.

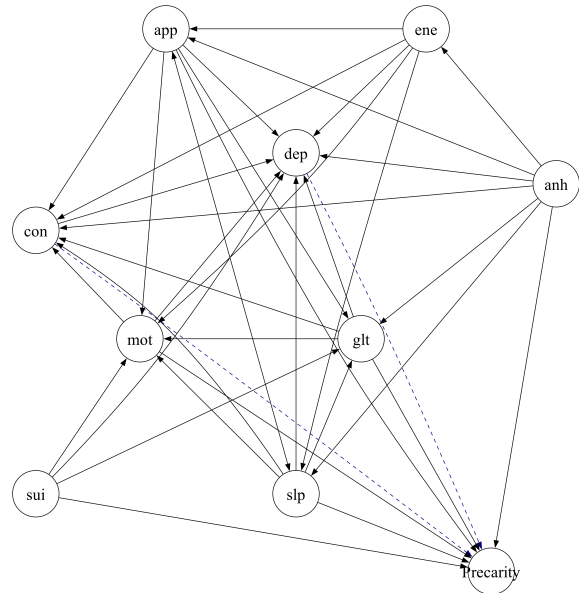


Figure 15: Resulting graphs of precariousness sum score and individual depression symptoms using PC.

6.6 Randomized Conditional Independence / Correlation Test (RCIT & RCoT)

RCIT (Randomized Conditional Independence Test) and RCoT (Randomized conditional Correlation Test) are advanced methods for scalable conditional independence (CI) testing, offering computational efficiency while maintaining the accuracy of kernel-based approaches. These methods evaluate conditional independence between two variables X and Y given a third variable Z while addressing computational challenges inherent in kernel-based CI tests. In this section, we provide a high-level overview of RCIT and RCoT based on (Strobl et al., 2019).

6.6.1 Kernel-Based Conditional Independence Testing

Traditional kernel-based CI tests, such as the Kernel Conditional Independence Test (KCIT), compute dependencies using the Hilbert-Schmidt Independence Criterion (HSIC) in reproducing kernel Hilbert spaces (RKHS) (Zhang et al., 2012). KCIT uses the following hypothesis framework:

$$H_0 : X \perp\!\!\!\perp Y | Z, \quad H_1 : X \not\perp\!\!\!\perp Y | Z.$$

The core quantity in KCIT is the partial cross-covariance operator:

$$\Sigma_{XY \cdot Z} = \Sigma_{XY} - \Sigma_{XZ} \Sigma_{ZZ}^{-1} \Sigma_{ZY},$$

where Σ_{XY} represents the cross-covariance operator between X and Y , and $\Sigma_{XZ} \Sigma_{ZZ}^{-1} \Sigma_{ZY}$ removes the dependence mediated by Z .

The squared Hilbert-Schmidt (HS) norm of $\Sigma_{XY \cdot Z}$ serves as the test statistic:

$$\|\Sigma_{XY \cdot Z}\|_{HS}^2 = 0 \quad \text{if and only if} \quad X \perp\!\!\!\perp Y | Z.$$

KCIT estimates residual dependencies using kernel ridge regression:

$$f^*(z) = K_Z(K_Z + \lambda I)^{-1} f(x),$$

where K_Z is the kernel matrix for Z , $f(x)$ is the kernel feature map for X , and λ is the ridge regularization parameter. The residual function for X is:

$$f_{\text{res}}(x) = f(x) - f^*(z) = R_Z f(x),$$

with:

$$R_Z = I - K_Z(K_Z + \lambda I)^{-1}.$$

The kernel matrix for residualized X is:

$$K_{X \cdot Z} = R_Z K_X R_Z,$$

and similarly for Y , $K_{Y \cdot Z} = R_Z K_Y R_Z$.

The test statistic is computed as:

$$T_{XY \cdot Z} = \frac{1}{n^2} \text{tr}(K_{X \cdot Z} K_{Y \cdot Z}),$$

which estimates the Hilbert-Schmidt (HS) norm of the partial cross-covariance operator. To ensure convergence, KCIT scales the statistic by n :

$$S_K = nT_{XY \cdot Z}.$$

The null hypothesis H_0 is rejected if S_K exceeds a threshold determined by permutation or moment-matching-based null distribution (Lindsay et al., 2000).

6.6.2 Random Fourier Features (RFFs)

Kernel-based methods like KCIT face scalability issues, as they involve operations on $n \times n$ kernel matrices, which scale quadratically with the sample size n . RCIT and RCoT overcome this bottleneck using *Random Fourier Features (RFFs)* to approximate kernel operations efficiently.

6.6.2.1 Bochner's Theorem

Bochner's theorem provides the foundation for RFFs, stating that any continuous shift-invariant kernel $k(x, y)$ can be expressed as:

$$k(x, y) = \int_{\mathbb{R}^p} e^{i\omega^\top(x-y)} dP_\omega,$$

where P_ω is the spectral distribution of the kernel. For the widely used RBF kernel:

$$k(x, y) = \exp\left(-\frac{\|x - y\|^2}{2\sigma^2}\right),$$

P_ω follows a Gaussian distribution: $\omega \sim \mathcal{N}(0, \sigma^2 I)$.

6.6.2.2 RFF Approximation

Using Monte Carlo sampling, the kernel function is approximated as:

$$k(x, y) \approx \phi(x)^\top \phi(y),$$

where $\phi(x)$ is the random Fourier feature mapping:

$$\phi(x) = \sqrt{\frac{2}{D}} \cos(W^\top x + b),$$

with $W \sim \mathcal{N}(0, \sigma^2 I)$ and $b \sim \text{Uniform}(0, 2\pi)$. Here, D is the number of Fourier features, which balances computational efficiency and approximation accuracy.

6.6.3 Differences Between RCIT and RCoT

RCIT and RCoT differ in their test statistics, computational efficiency, and practical performance, which makes them suited for different scenarios in causal discovery. RCIT evaluates the Hilbert-Schmidt norm of the full partial cross-covariance operator, providing a general test for conditional independence but at a higher

computational cost. RCoT simplifies the process by using the Frobenius norm of a finite-dimensional residualized cross-covariance matrix, significantly reducing complexity and improving scalability.

These distinctions are particularly important for large-scale datasets, where RCoT's computational efficiency makes it a practical choice for high-dimensional causal discovery tasks.

6.6.3.1 RCIT: Randomized Conditional Independence Test

RCIT tests full conditional independence by examining the squared Hilbert-Schmidt (HS) norm of the partial cross-covariance operator $\Sigma_{XY \cdot Z}$:

$$S_K = nT_{XY \cdot Z} = \frac{1}{n} \text{tr}(K_{X \cdot Z} K_{Y \cdot Z}),$$

where $T_{XY \cdot Z}$ is an empirical estimate of $\|\Sigma_{XY \cdot Z}\|_{HS}^2$. The null and alternative hypotheses are:

$$H_0 : \|\Sigma_{XY \cdot Z}\|_{HS}^2 = 0, \quad H_1 : \|\Sigma_{XY \cdot Z}\|_{HS}^2 > 0.$$

RCIT is a general test for conditional independence but becomes computationally demanding as the size of Z increases, due to the high-dimensional kernel operations required.

6.6.3.2 RCoT: Randomized Conditional Correlation Test

RCoT simplifies the testing process by using a finite-dimensional partial cross-covariance matrix, avoiding full HS norm calculations. Instead, it uses the Frobenius norm of the residualized cross-covariance matrix:

$$S' = n\|C_{AB \cdot C}\|_F^2,$$

where $C_{AB \cdot C}$ represents the residualized cross-covariance matrix. The hypotheses are:

$$H_0 : \|C_{AB \cdot C}\|_F^2 = 0, \quad H_1 : \|C_{AB \cdot C}\|_F^2 > 0.$$

RCoT is computationally efficient and well-suited for large conditioning sets ($|Z| \geq 4$). Its simplicity enables robust calibration of the null distribution and improved scalability for high-dimensional data.

6.7 Analytical Calibration of the Linear Feedback Model

We consider a continuous-time, linear stochastic differential equation (SDE) model describing the coupled dynamics between depression (D) and social precariousness (P), each influenced by an external stressor (S). The system is specified as:

$$\begin{aligned} \frac{dD}{dt} &= \alpha_{DS}S + \alpha_{DP}P - D + \sigma_D \cdot \eta_D(t), \\ \frac{dP}{dt} &= \alpha_{PS}S + \alpha_{PD}D - P + \sigma_P \cdot \eta_P(t), \end{aligned}$$

where:

- S is a fixed or exogenous input (external financial stress),
- α_{DP} represents the feedback from precariousness to depression,
- α_{PD} represents the feedback from depression to precariousness,
- α_{DS} and α_{PS} capture the direct effects of S ,
- σ_D, σ_P are stochastic noise amplitudes,
- $\eta_D(t), \eta_P(t)$ are independent standard Wiener processes.

We fix the decay rates $\lambda_D = \lambda_P = 1$, normalizing the time scale due to lack of temporal resolution in the HELIUS dataset.

6.7.1 Stationarity Assumption

We assume the joint distribution of (D, P) reaches stationarity, leading to a multivariate Ornstein–Uhlenbeck process. Under this assumption, the system has a unique stationary distribution characterized by its covariance structure, which we match to the empirical data.

Let:

$$\Sigma_{DD} = \text{Var}(D), \quad \Sigma_{PP} = \text{Var}(P), \quad \Sigma_{SS} = \text{Var}(S),$$

$$\Sigma_{DP} = \text{Cov}(D, P), \quad \Sigma_{DS} = \text{Cov}(D, S), \quad \Sigma_{PS} = \text{Cov}(P, S).$$

From the HELIUS data, we use the following observed values:

$$\Sigma_{DD} = 1.000, \quad \Sigma_{PP} = 0.807, \quad \Sigma_{SS} = 0.743, \quad \Sigma_{DP} = 0.374, \quad \Sigma_{DS} = 0.357, \quad \Sigma_{PS} = 0.256.$$

6.7.2 Analytical Parameter Derivation

We consider a linear stochastic dynamical system in which depression (D) and social precariousness (P) evolve under mutual influence and are jointly affected by an exogenous stressor (S). We assume stationary dynamics governed by a two-dimensional Ornstein–Uhlenbeck process:

$$\begin{aligned} dD_t &= (-D_t + \alpha_{DP}P_t + \alpha_{DS}S_t) dt + \sigma_D dW_{1t}, \\ dP_t &= (-P_t + \alpha_{PD}D_t + \alpha_{PS}S_t) dt + \sigma_P dW_{2t}. \end{aligned}$$

Here, we fix the autoregressive decay rates to 1 for identifiability and treat α_{DP} — the influence of precariousness on depression — as a free parameter. All other parameters are then derived to ensure the model reproduces the empirical second-order moments: variances ($\Sigma_{DD}, \Sigma_{PP}, \Sigma_{SS}$) and covariances ($\Sigma_{DP}, \Sigma_{DS}, \Sigma_{PS}$).

Under the stationary solution of the linear SDE system, the following algebraic identities hold:

$$\begin{aligned}\Sigma_{DS} &= \alpha_{DS}\Sigma_{SS} + \alpha_{DP}\Sigma_{PS}, \\ \Sigma_{DP} &= \alpha_{DS}\Sigma_{PS} + \alpha_{DP}\Sigma_{PP}, \\ \Sigma_{PS} &= \alpha_{PS}\Sigma_{SS} + \alpha_{PD}\Sigma_{DS}.\end{aligned}$$

Solving these simultaneously yields the following closed-form expressions as functions of α_{DP} :

$$\begin{aligned}\alpha_{DS} &= \frac{\Sigma_{DS} - \alpha_{DP} \cdot \Sigma_{PS}}{\Sigma_{SS}}, \\ \alpha_{PD} &= \frac{2\Sigma_{DS}\Sigma_{PS} - 2\Sigma_{DP}\Sigma_{SS} - \alpha_{DP}\Sigma_{PS}^2 + \alpha_{DP}\Sigma_{PP}\Sigma_{SS}}{\Sigma_{DS}^2 - \Sigma_{DD}\Sigma_{SS}}, \\ \alpha_{PS} &= \frac{\Sigma_{DS}^2\Sigma_{PS} + \Sigma_{PS}\Sigma_{DD}\Sigma_{SS} + \Sigma_{DS}(-2\Sigma_{DP}\Sigma_{SS} - \alpha_{DP}\Sigma_{PS}^2 + \alpha_{DP}\Sigma_{PP}\Sigma_{SS})}{\Sigma_{SS}(\Sigma_{DS}^2 - \Sigma_{DD}\Sigma_{SS})}.\end{aligned}$$

The noise amplitudes σ_D^2 and σ_P^2 are derived from the Lyapunov equation associated with the stationary covariance matrix. These yield:

$$\begin{aligned}\sigma_D^2 &= \frac{-2(\Sigma_{DS}^2 - \Sigma_{DD}\Sigma_{SS} - \Sigma_{DS}\Sigma_{PS}\alpha_{DP} + \Sigma_{DP}\Sigma_{SS}\alpha_{DP})}{\Sigma_{SS}}, \\ \sigma_P^2 &= \frac{K}{\Sigma_{SS}(\Sigma_{DD}\Sigma_{SS} - \Sigma_{DS}^2)},\end{aligned}$$

where

$$\begin{aligned}K &= 8\Sigma_{DP}\Sigma_{DS}\Sigma_{PS}\Sigma_{SS} - 4\Sigma_{DP}^2\Sigma_{SS}^2 - 2\Sigma_{DS}^2(\Sigma_{PS}^2 + \Sigma_{PP}\Sigma_{SS}) \\ &\quad + 2\Sigma_{DS}\Sigma_{PS}(\Sigma_{PS}^2 - \Sigma_{PP}\Sigma_{SS})\alpha_{DP} + 2\Sigma_{SS}(\Sigma_{PP}\Sigma_{SS} - \Sigma_{PS}^2)(\Sigma_{DD} + \Sigma_{DP}\alpha_{DP}).\end{aligned}$$

These expressions define a one-parameter family of structurally distinct yet observationally equivalent models, each exactly matching the empirical second-order statistics.

6.7.3 Constraints on α_{DP}

Although all expressions are algebraically valid for arbitrary real α_{DP} , admissibility requires that the resulting model remains meaningful and stable.

6.7.3.1 Positivity Constraints

To ensure interpretability, we require all effects and noise terms to be strictly positive:

$$\alpha_{DS} > 0, \quad \alpha_{PD} > 0, \quad \alpha_{PS} > 0, \quad \sigma_D^2 > 0, \quad \sigma_P^2 > 0.$$

Each of these is a function of α_{DP} , and thus these conditions restrict its allowable range. In particular:

- $\alpha_{PD} = 0$ when $\alpha_{DP} \approx 0.698$,
- $\alpha_{DS} = 0$ when $\alpha_{DP} \approx 1.39$,
- $\sigma_D^2 = 0$ when $\alpha_{DP} \approx 3.30$,
- $\sigma_P^2 = 0$ at a value given exactly by:

$$\alpha_{DP}^{(\sigma_P=0)} = \frac{-\Sigma_{DD}\Sigma_{PP}\Sigma_{SS}^2 + \Sigma_{DD}\Sigma_{PS}^2\Sigma_{SS} + 2\Sigma_{DP}^2\Sigma_{SS}^2 - 4\Sigma_{DP}\Sigma_{DS}\Sigma_{PS}\Sigma_{SS} + \Sigma_{DS}^2\Sigma_{PP}\Sigma_{SS} + \Sigma_{DS}^2\Sigma_{PS}^2}{\Sigma_{DP}\Sigma_{PP}\Sigma_{SS}^2 - \Sigma_{DP}\Sigma_{PS}^2\Sigma_{SS} - \Sigma_{DS}\Sigma_{PP}\Sigma_{PS}\Sigma_{SS} + \Sigma_{DS}\Sigma_{PS}^3}.$$

This value falls above $\alpha_{DP} = 0.698$, and thus does not tighten the admissible upper bound.

6.7.3.2 Stability Constraint

The system is stable if the deterministic dynamics converge, which requires the drift matrix

$$A = \begin{bmatrix} -1 & \alpha_{DP} \\ \alpha_{PD} & -1 \end{bmatrix}$$

to have all eigenvalues with negative real parts. This is equivalent to:

$$\text{Tr}(A) < 0 \quad \text{and} \quad \det(A) = 1 - \alpha_{DP}\alpha_{PD} > 0.$$

The trace condition is always satisfied ($\text{Tr}(A) = -2$), so stability reduces to:

$$\alpha_{DP} \cdot \alpha_{PD} < 1.$$

This condition fails exactly when $\alpha_{PD} \rightarrow 0^+$, which coincides with the tightest positivity constraint.

6.7.4 Admissible Range

Numerical evaluation using empirical covariances from the HELIUS dataset shows that:

- $\alpha_{PD} \rightarrow 0$ at $\alpha_{DP} \approx 0.698$,
- All other positivity and stability constraints are looser.

Hence, the maximum valid value is:

$$\alpha_{DP}^{\max} = 0.698$$

All simulations and model variants are confined to the admissible domain:

$$\alpha_{DP} \in [0, 0.698]$$

This guarantees that resulting systems are dynamically stable, fully positive, and consistent with empirical second-order moments.

Acknowledgements

The HELIUS study is conducted by the Amsterdam University Medical Centers, location AMC and the Public Health Service of Amsterdam. Both organisations provided core support for HELIUS. The HELIUS study is also funded by the Dutch Heart Foundation, the Netherlands Organization for Health Research and Development (ZonMw), the European Union (FP-7), and the European Fund for the Integration of non-EU immigrants (EIF). We are most grateful to the participants of the HELIUS study and the management team, research nurses, interviewers, research assistants and other staff who have taken part in gathering the data of this study.